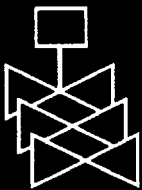
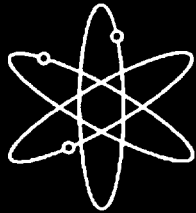
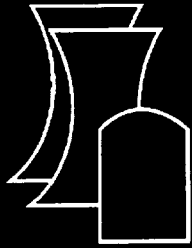


The Effect of Aging at 343°C on the Microstructure and Mechanical Properties of Type 308 Stainless Steel Weldments

Oak Ridge National Laboratory

U.S. Nuclear Regulatory Commission
Office of Nuclear Regulatory Research
Washington, DC 20555-0001



**AVAILABILITY OF REFERENCE MATERIALS
IN NRC PUBLICATIONS**

NRC Reference Material

As of November 1999, you may electronically access NUREG-series publications and other NRC records at NRC's Public Electronic Reading Room at www.nrc.gov/NRC/ADAMS/index.html.

Publicly released records include, to name a few, NUREG-series publications; *Federal Register* notices; applicant, licensee, and vendor documents and correspondence; NRC correspondence and internal memoranda; bulletins and information notices; inspection and investigative reports; licensee event reports; and Commission papers and their attachments.

NRC publications in the NUREG series, NRC regulations, and *Title 10, Energy*, in the Code of *Federal Regulations* may also be purchased from one of these two sources.

1. The Superintendent of Documents
U.S. Government Printing Office
P. O. Box 37082
Washington, DC 20402-9328
www.access.gpo.gov/su_docs
202-512-1800
2. The National Technical Information Service
Springfield, VA 22161-0002
www.ntis.gov
1-800-533-6847 or, locally, 703-805-6000

A single copy of each NRC draft report for comment is available free, to the extent of supply, upon written request as follows:

Address: Office of the Chief Information Officer,
Reproduction and Distribution
Services Section
U.S. Nuclear Regulatory Commission
Washington, DC 20555-0001

E-mail: DISTRIBUTION@nrc.gov

Facsimile: 301-415-2289

Some publications in the NUREG series that are posted at NRC's Web site address www.nrc.gov/NRC/NUREGS/indexnum.html are updated periodically and may differ from the last printed version. Although references to material found on a Web site bear the date the material was accessed, the material available on the date cited may subsequently be removed from the site.

Non-NRC Reference Material

Documents available from public and special technical libraries include all open literature items, such as books, journal articles, and transactions, *Federal Register* notices, Federal and State legislation, and congressional reports. Such documents as theses, dissertations, foreign reports and translations, and non-NRC conference proceedings may be purchased from their sponsoring organization.

Copies of industry codes and standards used in a substantive manner in the NRC regulatory process are maintained at—

The NRC Technical Library
Two White Flint North
11545 Rockville Pike
Rockville, MD 20852-2738

These standards are available in the library for reference use by the public. Codes and standards are usually copyrighted and may be purchased from the originating organization or, if they are American National Standards, from—

American National Standards Institute
11 West 42nd Street
New York, NY 10036-8002
www.ansi.org
212-642-4900

The NUREG series comprises (1) technical and administrative reports and books prepared by the staff (NUREG-XXXX) or agency contractors (NUREG/CR-XXXX), (2) proceedings of conferences (NUREG/CP-XXXX), (3) reports resulting from international agreements (NUREG/IA-XXXX), (4) brochures (NUREG/BR-XXXX), and (5) compilations of legal decisions and orders of the Commission and Atomic and Safety Licensing Boards and of Directors' decisions under Section 2.206 of NRC's regulations (NUREG-0750).

DISCLAIMER: This report was prepared as an account of work sponsored by an agency of the U.S. Government. Neither the U.S. Government nor any agency thereof, nor any employee, makes any warranty, expressed or implied, or assumes any legal liability or responsibility for any third party's use, or the results of such use, of any information, apparatus, product, or process disclosed in this publication, or represents that its use by such third party would not infringe privately owned rights.

The Effect of Aging at 343°C on the Microstructure and Mechanical Properties of Type 308 Stainless Steel Weldments

Manuscript Completed: May 1999
Date Published: November 2000

Prepared by
D. J. Alexander, K. B. Alexander,
M. K. Miller, R. K. Nanstad

Y. A. Davidov, Visiting Scientist
Institute for Metal Science
Bulgaria

Oak Ridge National Laboratory
Managed by Lockheed Martin Energy Research Corp.

Oak Ridge National Laboratory
Oak Ridge, TN 37831-6151

C. J. Fairbanks, NRC Project Manager

Prepared for
Division of Engineering Technology
Office of Nuclear Regulatory Research
U.S. Nuclear Regulatory Commission
Washington, DC 20555-0001
NRC Job Code W6953



**NUREG/CR-6628 has been reproduced
from the best available copy.**

ABSTRACT

Some piping systems in light-water reactors contain welds made with type 308 stainless steel filler metal that are routinely subjected to operating temperatures above 300°C. The effect of long-term aging of stainless steel welds at 343°C (650°F) has been studied by the Heavy-Section Steel Irradiation Program to determine the extent of degradation of the mechanical properties of the weld metal. Three multipass shielded metal-arc welds were prepared from type 304L base plate with type 308 filler metal. The chemistry of the filler wire was adjusted to obtain different ferrite levels (4, 8, or 12%). Portions of these welds were aged for 3,000, 10,000, 20,000 or 50,000 h at 343°C. Charpy V-notch and tensile specimens were taken from both the tops and the bottoms of these welds. The tensile results were similar for all the specimens and showed little effect of aging on the yield or ultimate tensile strength or the ductility. In contrast, the Charpy impact toughness, as characterized by either the ductile-to-brittle transition temperature or the upper-shelf energy, was significantly degraded by aging. The extent of the degradation increased with increasing ferrite content and increasing aging time. Embrittlement continued to increase up to 50,000 h of aging with no indication of a saturation. At lower test temperatures the fracture path appeared to preferentially follow the ferrite phase, which fractured by a brittle cleavage-like mode. Sections taken perpendicular to the fracture plane revealed microcracks in the ferrite and strain-induced martensite in the austenite phase near the fracture surface. Aging for 50,000 h at 343°C also resulted in a significant decrease in the J-Integral fracture toughness at 290°C of the 8 and 12% ferrite welds. The microstructures of the welds were examined by optical metallography, scanning and transmission electron microscopy, and atom probe field-ion microscopy. Examination of material aged for 20,000 h showed that the ferrite phase undergoes spinodal decomposition, creating iron-rich and chromium-rich regions. Additionally, relatively large G-phase particles were observed heterogeneously associated with dislocations, and fine G-phase particles were distributed homogeneously through the ferrite phase. No changes were observed in the austenite phase. The hardening of the ferrite phase due to the spinodal decomposition is believed to be the primary factor responsible for the loss of toughness observed after aging.

CONTENTS

ABSTRACT	iii
LIST OF FIGURES	vii
LIST OF TABLES	xi
ACKNOWLEDGMENTS	xiii
FOREWORD	xv
INTRODUCTION	1
EXPERIMENTAL PROCEDURES	2
RESULTS	5
Mechanical Properties	6
Microstructural Observations	10
DISCUSSION	27
Fracture Toughness Testing	37
CONCLUSIONS	40
REFERENCES	41

LIST OF FIGURES

Figure	Page
1 Typical microstructures of the three weld metals. Left, 4% ferrite; middle, 8% ferrite; right 12% ferrite	6
2 Average yield and ultimate tensile strengths for type 308 stainless steel weld materials aged at 343°C	7
3 Effect of aging at 343°C on Charpy impact transition curves for type 308 stainless steel weld materials, 4% ferrite	8
4 Effect of aging at 343°C on Charpy impact transition curves for type 308 stainless steel weld materials, 8% ferrite	9
5 Effect of aging at 343°C on Charpy impact transition curves for type 308 stainless steel weld materials, 12% ferrite	9
6 Effects of aging at 343°C on the impact properties of type 308 stainless steel weld metal. (a) Transition temperature versus aging time, and (b) upper-shelf energy versus aging time	11
7 Effects of aging at 343°C on the lateral expansion properties of type 308 stainless steel weld metal. (a) Transition temperature as measured at a lateral expansion of 0.89 mm (0.035 in.), and (b) lateral expansion upper-shelf value	12
8 Microstructure from the top of the type 308 stainless steel weld, 12% ferrite material, aged at 343°C for 20,000 h. Note the absence of carbide particles along the ferrite-austenite interfaces and the spherical MnSi particles	13
9 Microstructure from the middle of the type 308 stainless steel weld, 12% ferrite, aged at 343°C for 20,000 h. Note the carbides along many of the ferrite-austenite interfaces and the spherical MnSi particles	14
10 $M_{23}C_6$ carbides at the austenite-ferrite interphase boundaries of the type 308 stainless steel weld, 12% ferrite, aged at 343°C for 20,000 h. Left: view of cuboidal particles; right: diffraction pattern showing cube-on-cube orientation relationship of carbides with austenite matrix	16
11 Chromium and nickel composition profiles of the type 308 stainless steel 12% ferrite weld aged at 343°C for 20,000 h. (a) Obtained from EDS analysis, and (b) obtained from atom probe	17

12	Character plot showing segregation of carbon and phosphorus at the austenite/ferrite interface of the 12% ferrite weld, aged at 343°C for 20,000 h. The character definitions are given, and the interface regions are marked by the arrows	18
13	G-phase precipitation in 12% ferrite weld after 20,000 h at 343°C. (a) Bright-field micrograph, (b) $(333)_G$ dark-field micrograph, and (c) weak-beam micrograph showing dislocation	19
14	G-phase precipitation in 12% ferrite weld after 20,000 h at 343°C. (a) Diffraction pattern from a $(1\bar{1}0)$ zone axis in the ferrite showing G-phase reflections, and (b) superimposed G-phase and ferrite $(1\bar{1}0)$ simulated diffraction patterns. Only the most intense reflections are shown	21
15	Bright-field micrograph of G-phase precipitation in 12% ferrite weld after 20,000 h at 343°C. The arrows indicate large G-phase precipitates associated with dislocations. G-phase precipitates (dark) are also observed in the matrix	22
16	Bright-field micrograph of the ferrite-austenite interphase boundary in the 12% ferrite weld showing the mottled appearance of the ferrite (left) after aging 20,000 h at 343°C. Such a mottled appearance is frequently associated with spinodal decomposition. Note the absence of mottling in the austenite phase (right)	23
17	Field ion micrograph of the 12% ferrite weld aged 20,000 h at 343°C, showing brightly imaging ultrafine G-phase precipitates in the ferrite phase	24
18	Atom probe chromium composition profiles of the 12% ferrite weld using a 50-ion block size, through the (a) unaged ferrite and the (b) ferrite aged at 343°C for 20,000 h. Phase separation into iron-rich and chromium-enriched regions is evident in (b), showing larger chromium deviations	25
19	Fractography of type 308 stainless steel weld metal specimen tested on upper shelf. Left: low-magnification view showing rugged fracture surface; right: higher magnification showing ductile microvoid coalescence; 12% ferrite, unaged, tested at 100°C	28
20	Fractography of type 308 stainless steel weld metal specimen tested in transition regime. Left: low-magnification view showing stepped appearance of fracture surface; right: higher magnification view showing flat regions with cleavage-like appearance. 12% ferrite material, aged at 343°C for 20,000 h, tested at -50°C	29

21	Section perpendicular to the fracture surface of a type 308 stainless steel weld metal Charpy impact specimen showing microcracks associated with the ferrite regions. Left: optical view of section, with microcracks indicated by arrows; right: higher-magnification SEM micrograph showing detail of microcrack in ferrite. 12% ferrite material, aged 343°C for 20,000 h, tested at -50°C	33
22	The effects of a reversion heat treatment (550°C for 1 h, water quench) on the impact properties of (a) 8% ferrite material and (b) 12% ferrite material, of type 308 stainless steel weld metal. Aging was performed at 343°C	35
23	Effects of aging at 343°C on the J-Integral fracture toughness of type 308 stainless steel weld metal. All tests conducted with precracked Charpy V-notch specimens at 290°C	38

LIST OF TABLES

Table	Page
1 Chemical composition of the three type 308 stainless steel weld materials (4, 8, and 12% ferrite content)	5
2 Charpy impact properties of the three type 308 stainless steel weld materials (4, 8, and 12% ferrite content)	10
3 Compositions of austenite and ferrite aged for 20,000 h at 343°C determined using atom probe field-ion microscopy	19
4 Statistical analysis of atom probe data (same specimens as in Table 3)	26
5 Effects of aging at 343°C for 50,000 h on fracture toughness of type 308 weld metal	38

ACKNOWLEDGMENTS

The authors would like to thank J. F. King of the Materials Joining Group at ORNL, who was responsible for the fabrication of the welds; M. G. Hetherington of Oxford University (posthumously) for providing the sample distribution analysis software; J. J. Henry, Jr., and E. T. Manneschildt for experimental assistance; and S. G. Druce and J. Bentley for helpful discussions. This work was supported by the NRC Heavy-Section Steel Irradiation Program and the Division of Materials Sciences, U.S. Department of Energy, under contract DE-AC05-96OR22464 with Lockheed Martin Energy Research Corp.

FOREWORD

The work reported here was performed at the Oak Ridge National Laboratory (ORNL) under the Heavy-Section Steel Irradiation (HSSI) Program, T. M. Rosseel, Program Manager. The program is sponsored by the Office of Nuclear Regulatory Research of the U.S. Nuclear Regulatory Commission (NRC). The technical monitor for the NRC is C. J. Fairbanks.

This report is designated HSSI Report 23. Reports in this series are listed below:

1. F. M. Haggag, W. R. Corwin, and R. K. Nanstad, Martin Marietta Energy Systems, Inc., Oak Ridge Natl. Lab., Oak Ridge, Tenn., *Irradiation Effects on Strength and Toughness of Three-Wire Series-Arc Stainless Steel Weld Overlay Cladding*, USNRC Report NUREG/CR-5511 (ORNL/TM-11439), February 1990.
2. L. F. Miller, C. A. Baldwin, F. W. Stallman, and F. B. K. Kam, Martin Marietta Energy Systems, Inc., Oak Ridge Natl. Lab., Oak Ridge, Tenn., *Neutron Exposure Parameters for the Metallurgical Test Specimens in the Sixth Heavy-Section Steel Irradiation Series*, USNRC Report NUREG/CR-5409 (ORNL/TM-11267), March 1990.
3. S. K. Iskander, W. R. Corwin, and R. K. Nanstad, Martin Marietta Energy Systems, Inc., Oak Ridge Natl. Lab., Oak Ridge, Tenn., *Results of Crack-Arrest Tests on Two Irradiated High-Copper Welds*, USNRC Report NUREG/CR-5584 (ORNL/TM-11575), December 1990.
4. R. K. Nanstad and R. G. Berggren, Martin Marietta Energy Systems, Inc., Oak Ridge Natl. Lab., Oak Ridge, Tenn., *Irradiation Effects on Charpy Impact and Tensile Properties of Low Upper-Shelf Welds, HSSI Series 2 and 3*, USNRC Report NUREG/CR-5696 (ORNL/TM-11804), August 1991.
5. R. E. Stoller, Martin Marietta Energy Systems, Inc., Oak Ridge Natl. Lab., Oak Ridge, Tenn., *Modeling the Influence of Irradiation Temperature and Displacement Rate on Radiation-Induced Hardening in Ferritic Steels*, USNRC Report NUREG/CR5859 (ORNL/TM-12073), August 1992.
6. R. K. Nanstad, D. E. McCabe, and R. L. Swain, Martin Marietta Energy Systems, Inc., Oak Ridge Natl. Lab., Oak Ridge, Tenn., *Chemical Composition RT_{NDT} Determinations for Midland Weld WF-70*, USNRC Report NUREG/CR-5914 (ORNL-6740), December 1992.
7. R. K. Nanstad, F. M. Haggag, D. E. McCabe, S. K. Iskander, K. O. Bowman, and B. H. Menke, Martin Marietta Energy Systems, Inc., Oak Ridge Natl. Lab., Oak Ridge, Tenn., *Irradiation Effects on Fracture Toughness of Two High-Copper Submerged-Arc Welds*, USNRC Report NUREG/CR-5913 (ORNL/TM-12156/V1), October 1992.
8. S. K. Iskander, W. R. Corwin, and R. K. Nanstad, Martin Marietta Energy Systems, Inc., Oak Ridge Natl. Lab., Oak Ridge, Tenn., *Crack-Arrest Tests on Two Irradiated High-Copper Welds*, USNRC Report NUREG/CR-6139 (ORNL/TM-12513), March 1994.

9. R. E. Stoller, Martin Marietta Energy Systems, Inc., Oak Ridge Natl. Lab., Oak Ridge, Tenn., *A Comparison of the Relative Importance of Copper Precipitates and Point Defects in Reactor Pressure Vessel Embrittlement*, USNRC Report NUREG/CR-6231 (ORNL/TM-6811), December 1994.
10. D. E. McCabe, R. K. Nanstad, S. K. Iskander, and R. L. Swain, Martin Marietta Energy Systems, Inc., Oak Ridge Natl. Lab., Oak Ridge, Tenn., *Unirradiated Material Properties of Midland Weld WF-70*, USNRC Report NUREG/CR-6249 (ORNL/TM-12777), October 1994.
11. P. M. Rice and R. E. Stoller, Lockheed Martin Energy Systems, Oak Ridge Natl. Lab., Oak Ridge, Tenn., *Microstructural Characterization of Selected AEA/UCSB Model FeCuMn Alloys*, USNRC Report NUREG/CR-6332 (ORNL/TM-12980), June 1996.
12. J. H. Giovanola and J. E. Crocker, SRI International, *Fracture Toughness Testing with Cracked Round Bars: Feasibility Study*, USNRC Report NUREG/CR-6342 (ORNL/SUB/94-DHK60), to be published.
13. F. M. Haggag and R. K. Nanstad, Lockheed Martin Energy Systems, Oak Ridge Natl. Lab., Oak Ridge, Tenn., *Effects of Thermal Aging and Neutron Irradiation on the Mechanical Properties of Three-Wire Stainless Steel Weld Overlay Cladding*, USNRC Report NUREG/CR-6363 (ORNL/TM-13047), May 1997.
14. M. A. Sokolov and D. J. Alexander, Lockheed Martin Energy Systems, Oak Ridge Natl. Lab., Oak Ridge, Tenn., *An Improved Correlation Procedure for Subsize and Full-Size Charpy Impact Specimen Data*, USNRC Report NUREG/CR-6379 (ORNL/TM-13088), March 1997.
15. S. K. Iskander and R. E. Stoller, Lockheed Martin Energy Research Corporation, Oak Ridge Natl. Lab., Oak Ridge, Tenn., *Results of Charpy V-Notch Impact Testing of Structural Steel Specimens Irradiated at $\sim 30^{\circ}\text{C}$ to 1×10^6 neutrons/cm² in a Commercial Reactor Cavity*, USNRC Report NUREG/CR-6399 (ORNL-6886), April 1997.
16. S. K. Iskander, P. P. Milella, and A. Pini, Lockheed Martin Energy Research Corporation, Oak Ridge Natl. Lab., Oak Ridge, Tenn., *Results of Crack-Arrest Tests on Irradiated A 503 Class 3 Steel*, USNRC Report NUREG/CR-6447 (ORNL-6894), February 1998.
17. P. Pareige, K. F. Russell, R. E. Stoller, and M. K. Miller, Lockheed Martin Energy Research Corporation, Oak Ridge Natl. Lab., Oak Ridge, Tenn., *Influence of Long-Term Thermal Aging on the Microstructural Evolution of Nuclear Reactor Pressure Vessel Materials: An Atom Probe Study*, USNRC Report NUREG/CR-6537(ORNL-13406), March 1998.
18. I. Remec, C. A. Baldwin, and F. B. K. Kam, Lockheed Martin Energy Research Corporation, Oak Ridge Natl. Lab., Oak Ridge, Tenn., *Neutron Exposure Parameters for Capsule 10.05 in the Heavy-Section Steel Irradiation Program Tenth Irradiation Series*, USNRC Report NUREG/CR-6600 (ORNL/TM-13548), October 1998.

19. I. Remec, C. A. Baldwin, and F. B. K. Kam, Lockheed Martin Energy Research Corporation, Oak Ridge Natl. Lab., Oak Ridge, Tenn., *Neutron Exposure Parameters for the Dosimetry Capsule in the Heavy-Section Steel Irradiation Program Tenth Irradiation Series*, USNRC Report NUREG/CR-6601 (ORNL/TM-13549), October 1998.
20. D. E. McCabe, R. K. Nanstad, S. K. Iskander, D. W. Heatherly, and R. L. Swain, Lockheed Martin Energy Research Corporation, Oak Ridge Natl. Lab., Oak Ridge, Tenn., *Evaluation of WF-70 Weld Metal from the Midland Unit 1 Reactor Vessel—Final Report*, USNRC Report NUREG/CR-5736 (ORNL/TM-13748), to be published.
21. Mikhail A. Sokolov and Randy K. Nanstad, Lockheed Martin Energy Research Corporation, Oak Ridge Natl. Lab., Oak Ridge, Tenn., *Comparison of Irradiation-Induced Shifts of K_{Jc} and Charpy Impact Toughness for Reactor Pressure Vessel Steels*, USNRC Report NUREG/CR-6609 (ORNL/TM-13755), to be published.
22. S. K. Iskander, C. A. Baldwin, D. W. Heatherly, D. E. McCabe, I. Remec, and R. L. Swain, Lockheed Martin Energy Research Corporation, Oak Ridge Natl. Lab., Oak Ridge, Tenn., *Detailed Results of Testing Unirradiated and Irradiated Crack-Arrest Toughness Specimens from the Low Upper-Shelf Energy, High Copper Weld, WF-70*, USNRC Report NUREG/CR-6621 (ORNL/TM-13764), to be published.
23. This report.

The HSSI Program includes both follow-on and the direct continuation of work that was performed under the Heavy-Section Steel Technology (HSST) Program. Previous HSST reports related to irradiation effects in pressure vessel materials and those containing unirradiated properties of materials used in HSSI and HSST irradiation programs are tabulated below as a convenience to the reader.

C. E. Childress, Union Carbide Corp. Nuclear Div., Oak Ridge Natl. Lab., Oak Ridge, Tenn., *Fabrication History of the First Two 12-in.-Thick A-533 Grade B, Class 1 Steel Plates of the Heavy-Section Steel Technology Program*, ORNL-4313, February 1969.

T. R. Mager and F. O. Thomas, Westinghouse Electric Corporation, PWR Systems Division, Pittsburgh, Pa., *Evaluation by Linear Elastic Fracture Mechanics of Radiation Damage to Pressure Vessel Steels*, WCAP-7328 (Rev.), October 1969.

P. N. Randall, TRW Systems Group, Redondo Beach, Calif., *Gross Strain Measure of Fracture Toughness of Steels*, HSSTP-TR-3, Nov. 1, 1969.

L. W. Loechel, Martin Marietta Corporation, Denver, Colo., *The Effect of Testing Variables on the Transition Temperature in Steel*, MCR-69-189, Nov. 20, 1969.

W. O. Shabbits, W. H. Pryle, and E. T. Wessel, Westinghouse Electric Corporation, PWR Systems Division, Pittsburgh, Pa., *Heavy-Section Fracture Toughness Properties of A533 Grade B Class 1 Steel Plate and Submerged Arc Weldment*, WCAP-7414, December 1969.

- C. E. Childress, Union Carbide Corp. Nuclear Div., Oak Ridge Natl. Lab., Oak Ridge, Tenn., *Fabrication History of the Third and Fourth ASTM A-533 Steel Plates of the Heavy-Section Steel Technology Program*, ORNL-4313-2, February 1970.
- P. B. Crosley and E. J. Ripling, Materials Research Laboratory, Inc., Glenwood, Ill., *Crack Arrest Fracture Toughness of A533 Grade B Class 1 Pressure Vessel Steel*, HSSTP-TR-8, March 1970.
- F. J. Loss, Naval Research Laboratory, Washington, D.C., *Dynamic Tear Test Investigations of the Fracture Toughness of Thick-Section Steel*, NRL-7056, May 14, 1970.
- T. R. Mager, Westinghouse Electric Corporation, PWR Systems Division, Pittsburgh, Pa., *Post-Irradiation Testing of 2T Compact Tension Specimens*, WCAP-7561, August 1970.
- F. J. Witt and R. G. Berggren, Union Carbide Corp. Nuclear Div., Oak Ridge Natl. Lab., Oak Ridge, Tenn., *Size Effects and Energy Disposition in Impact Specimen Testing of ASTM A533 Grade B Steel*, ORNL/TM-3030, August 1970.
- D. A. Canonico, Union Carbide Corp. Nuclear Div., Oak Ridge Natl. Lab., Oak Ridge, Tenn., *Transition Temperature Considerations for Thick-Wall Nuclear Pressure Vessels*, ORNL/TM-3114, October 1970.
- T. R. Mager, Westinghouse Electric Corporation, PWR Systems Division, Pittsburgh, Pa., *Fracture Toughness Characterization Study of A533, Grade B, Class 1 Steel*, WCAP-7578, October 1970.
- W. O. Shabbits, Westinghouse Electric Corporation, PWR Systems Division, Pittsburgh, Pa., *Dynamic Fracture Toughness Properties of Heavy-Section A533 Grade B Class 1 Steel Plate*, WCAP-7623, December 1970.
- C. E. Childress, Union Carbide Corp. Nuclear Div., Oak Ridge Natl. Lab., Oak Ridge, Tenn., *Fabrication Procedures and Acceptance Data for ASTM A-533 Welds and a 10-in.-Thick ASTM A-543 Plate of the Heavy Section Steel Technology Program*, ORNL-TM-4313-3, January 1971.
- D. A. Canonico and R. G. Berggren, Union Carbide Corp. Nuclear Div., Oak Ridge Natl. Lab., Oak Ridge, Tenn., *Tensile and Impact Properties of Thick-Section Plate and Weldments*, ORNL/TM-3211, January 1971.
- C. W. Hunter and J. A. Williams, Hanford Eng. Dev. Lab., Richland, Wash., *Fracture and Tensile Behavior of Neutron-Irradiated A533-B Pressure Vessel Steel*, HEDL-TME-71-76, Feb. 6, 1971.
- C. E. Childress, Union Carbide Corp. Nuclear Div., Oak Ridge Natl. Lab., Oak Ridge, Tenn., *Manual for ASTM A533 Grade B Class 1 Steel (HSST Plate 03) Provided to the International Atomic Energy Agency*, ORNL/TM-3193, March 1971.

- P. N. Randall, TRW Systems Group, Redondo Beach, Calif., *Gross Strain Crack Tolerance of A533-B Steel*, HSSTP-TR-14, May 1, 1971.
- C. L. Segaser, Union Carbide Corp. Nuclear Div., Oak Ridge Natl. Lab., Oak Ridge, Tenn., *Feasibility Study, Irradiation of Heavy-Section Steel Specimens in the South Test Facility of the Oak Ridge Research Reactor*, ORNL/TM-3234, May 1971.
- H. T. Corten and R. H. Sailors, University of Illinois, Urbana, Ill., *Relationship Between Material Fracture Toughness Using Fracture Mechanics and Transition Temperature Tests*, T&AM Report 346, Aug. 1, 1971.
- L. A. James and J. A. Williams, Hanford Eng. Dev. Lab., Richland, Wash., *Heavy Section Steel Technology Program Technical Report No. 21, The Effect of Temperature and Neutron Irradiation Upon the Fatigue-Crack Propagation Behavior of ASTM A533 Grade B, Class 1 Steel*, HEDL-TME 72-132, September 1972.
- P. B. Crosley and E. J. Ripling, Materials Research Laboratory, Inc., Glenwood, Ill., *Crack Arrest in an Increasing K-Field*, HSSTP-TR-27, January 1973.
- W. J. Stelzman and R. G. Berggren, Union Carbide Corp. Nuclear Div., Oak Ridge Natl. Lab., Oak Ridge, Tenn., *Radiation Strengthening and Embrittlement in Heavy-Section Steel Plates and Welds*, ORNL-4871, June 1973.
- J. M. Steichen and J. A. Williams, Hanford Eng. Dev. Lab., Richland, Wash., *High Strain Rate Tensile Properties of Irradiated ASTM A533 Grade B Class 1 Pressure Vessel Steel*, HEDL-TME 73-74, July 1973.
- J. A. Williams, Hanford Eng. Dev. Lab., Richland, Wash., *The Irradiation and Temperature Dependence of Tensile and Fracture Properties of ASTM A533, Grade B, Class 1 Steel Plate and Weldment*, HEDL-TME 73-75, August 1973.
- J. A. Williams, Hanford Eng. Dev. Lab., Richland, Wash., *Some Comments Related to the Effect of Rate on the Fracture Toughness of Irradiated ASTM A553-B Steel Based on Yield Strength Behavior*, HEDL-SA 797, December 1974.
- J. A. Williams, Hanford Eng. Dev. Lab., Richland, Wash., *The Irradiated Fracture Toughness of ASTM A533, Grade B, Class 1 Steel Measured with a Four-Inch-Thick Compact Tension Specimen*, HEDL-TME 75-10, January 1975.
- J. G. Merkle, G. D. Whitman, and R. H. Bryan, Union Carbide Corp. Nuclear Div., Oak Ridge Natl. Lab., Oak Ridge, Tenn., *An Evaluation of the HSST Program Intermediate Pressure Vessel Tests in Terms of Light-Water-Reactor Pressure Vessel Safety*, ORNL/TM-5090, November 1975.
- J. A. Davidson, L. J. Ceschini, R. P. Shogan, and G. V. Rao, Westinghouse Electric Corporation, Pittsburgh, Pa., *The Irradiated Dynamic Fracture Toughness of ASTM A533, Grade B, Class 1 Steel Plate and Submerged Arc Weldment*, WCAP-8775, October 1976.

- J. A. Williams, Hanford Eng. Dev. Lab., Richland, Wash., *Tensile Properties of Irradiated and Unirradiated Welds of A533 Steel Plate and A508 Forgings*, NUREG/CR-1158 (ORNL/SUB-79/50917/2), July 1979.
- J. A. Williams, Hanford Eng. Dev. Lab., Richland, Wash., *The Ductile Fracture Toughness of Heavy-Section Steel Plate*, NUREG/CR-0859, September 1979.
- K. W. Carlson and J. A. Williams, Hanford Eng. Dev. Lab., Richland, Wash., *The Effect of Crack Length and Side Grooves on the Ductile Fracture Toughness Properties of ASTM A533 Steel*, NUREG/CR-1171 (ORNL/SUB-79/50917/3), October 1979.
- G. A. Clarke, Westinghouse Electric Corp., Pittsburgh, Pa., *An Evaluation of the Unloading Compliance Procedure for J-Integral Testing in the Hot Cell, Final Report*, NUREG/CR-1070 (ORNL/SUB-7394/1), October 1979.
- P. B. Crosley and E. J. Ripling, Materials Research Laboratory, Inc., Glenwood, Ill., *Development of a Standard Test for Measuring K_{Ia} with a Modified Compact Specimen*, NUREG/CR-2294 (ORNL/SUB-81/7755/1), August 1981.
- H. A. Domian, Babcock and Wilcox Company, Alliance, Ohio, *Vessel V-8 Repair and Preparation of Low Upper-Shelf Weldment*, NUREG/CR-2676 (ORNL/SUB/81-85813/1), June 1982.
- R. D. Cheverton, S. K. Iskander, and D. G. Ball, Union Carbide Corp. Nuclear Div., Oak Ridge Natl. Lab., Oak Ridge, Tenn., *PWR Pressure Vessel Integrity During Overcooling Accidents: A Parametric Analysis*, NUREG/CR-2895 (ORNL/TM-7931), February 1983.
- J. G. Merkle, Union Carbide Corp. Nuclear Div., Oak Ridge Natl. Lab., Oak Ridge, Tenn., *An Examination of the Size Effects and Data Scatter Observed in Small Specimen Cleavage Fracture Toughness Testing*, NUREG/CR-3672 (ORNL/TM-9088), April 1984.
- W. R. Corwin, Martin Marietta Energy Systems, Inc., Oak Ridge Natl. Lab., Oak Ridge, Tenn., *Assessment of Radiation Effects Relating to Reactor Pressure Vessel Cladding*, NUREG/CR-3671 (ORNL-6047), July 1984.
- W. R. Corwin, R. G. Berggren, and R. K. Nanstad, Martin Marietta Energy Systems, Inc., Oak Ridge Natl. Lab., Oak Ridge, Tenn., *Charpy Toughness and Tensile Properties of a Neutron Irradiated Stainless Steel Submerged-Arc Weld Cladding Overlay*, NUREG/CR-3927 (ORNL/TM-9709), September 1984.
- J. J. McGowan, Martin Marietta Energy Systems, Inc., Oak Ridge Natl. Lab., Oak Ridge, Tenn., *Tensile Properties of Irradiated Nuclear Grade Pressure Vessel Plate and Welds for the Fourth HSST Irradiation Series*, NUREG/CR-3978 (ORNL/TM-9516), January 1985.
- J. J. McGowan, Martin Marietta Energy Systems, Inc., Oak Ridge Natl. Lab., Oak Ridge, Tenn., *Tensile Properties of Irradiated Nuclear Grade Pressure Vessel Welds for the Third HSST Irradiation Series*, NUREG/CR-4086 (ORNL/TM-9477), March 1985.

W. R. Corwin, G. C. Robinson, R. K. Nanstad, J. G. Merkle, R. G. Berggren, G. M. Goodwin, R. L. Swain, and T. D. Owings, Martin Marietta Energy Systems, Inc., Oak Ridge Natl. Lab., Oak Ridge, Tenn., *Effects of Stainless Steel Weld Overlay Cladding on the Structural Integrity of Flawed Steel Plates in Bending, Series 1*, NUREG/CR-4015 (ORNL/TM-9390), April 1985.

W. J. Stelzman, R. G. Berggren, and T. N. Jones, Martin Marietta Energy Systems, Inc., Oak Ridge Natl. Lab., Oak Ridge, Tenn., *ORNL Characterization of Heavy-Section Steel Technology Program Plates 01, 02, and 03*, NUREG/CR-4092 (ORNL/TM-9491), April 1985.

G. D. Whitman, Martin Marietta Energy Systems, Inc., Oak Ridge Natl. Lab., Oak Ridge, Tenn., *Historical Summary of the Heavy-Section Steel Technology Program and Some Related Activities in Light-Water Reactor Pressure Vessel Safety Research*, NUREG/CR-4489 (ORNL-6259), March 1986.

R. H. Bryan, B. R. Bass, S. E. Bolt, J. W. Bryson, J. G. Merkle, R. K. Nanstad, and G. C. Robinson, Martin Marietta Energy Systems, Inc., Oak Ridge Natl. Lab., Oak Ridge, Tenn., *Test of 6-in.-Thick Pressure Vessels. Series 3: Intermediate Test Vessel V-8A — Tearing Behavior of Low Upper-Shelf Material*, NUREG-CR-4760 (ORNL-6187), May 1987.

D. B. Barker, R. Chona, W. L. Fournery, and G. R. Irwin, University of Maryland, College Park, Md., *A Report on the Round Robin Program Conducted to Evaluate the Proposed ASTM Standard Test Method for Determining the Plane Strain Crack Arrest Fracture Toughness, K_{Ia} , of Ferritic Materials*, NUREG/CR-4966 (ORNL/SUB/79-7778/4), January 1988.

L. F. Miller, C. A. Baldwin, F. W. Stallman, and F. B. K. Kam, Martin Marietta Energy Systems, Inc., Oak Ridge Natl. Lab., Oak Ridge, Tenn., *Neutron Exposure Parameters for the Metallurgical Test Specimens in the Fifth Heavy-Section Steel Technology Irradiation Series Capsules*, NUREG/CR-5019 (ORNL/TM-10582), March 1988.

J. J. McGowan, R. K. Nanstad, and K. R. Thoms, Martin Marietta Energy Systems, Inc., Oak Ridge Natl. Lab., Oak Ridge, Tenn., *Characterization of Irradiated Current-Practice Welds and A533 Grade B Class 1 Plate for Nuclear Pressure Vessel Service*, NUREG/CR-4880 (ORNL-6484/V1 and V2), July 1988.

R. D. Cheverton, W. E. Pennell, G. C. Robinson, and R. K. Nanstad, Martin Marietta Energy Systems, Inc., Oak Ridge Natl. Lab., Oak Ridge, Tenn., *Impact of Radiation Embrittlement on Integrity of Pressure Vessel Supports for Two PWR Plants*, NUREG/CR-5320 (ORNL/TM-10966), February 1989.

J. G. Merkle, Martin Marietta Energy Systems, Inc., Oak Ridge Natl. Lab., Oak Ridge, Tenn., *An Overview of the Low-Upper-Shelf Toughness Safety Margin Issue*, NUREG/CR-5552 (ORNL/TM-11314), August 1990.

R. D. Cheverton, T. L. Dickson, J. G. Merkle, and R. K. Nanstad, Martin Marietta Energy Systems, Inc., Oak Ridge Natl. Lab., Oak Ridge, Tenn., *Review of Reactor Pressure Vessel Evaluation Report for Yankee Rowe Nuclear Power Station (YAEC No. 1735)*, NUREG/CR-5799 (ORNL/TM-11982), March 1992.

The Effect of Aging at 343°C on the Microstructure and Mechanical Properties of Type 308 Stainless Steel Weldments¹

D. J. Alexander, K. B. Alexander,
M. K. Miller, R. K. Nanstad, and Y. A. Davidov

INTRODUCTION

Stainless steel is used extensively in the piping of light-water reactors (LWRs) and is routinely subjected to operating temperatures above 300°C. Frequently the piping systems contain welds made with type 308 stainless steel filler metal. Such welds typically contain significant amounts of ferrite to prevent hot cracking and to increase their strength. However, this ferrite may become embrittled after exposure to elevated temperatures. Therefore, the possibility of a degradation of the mechanical properties of these welds as a result of long-term aging at operating temperatures must be considered. Effects of aging at low temperatures have been studied extensively for duplex cast and wrought stainless steels (Refs. 1 and 2). In cast CF8-type materials, both G-phase precipitation and spinodal decomposition have been observed in the ferrite after aging in the temperature range of 300 to 400°C (Refs. 3–6). The extent of the decomposition was found to be strongly dependent on the overall alloy composition and the heat treatment. Higher-temperature agings (475°C) of type 308 and type 308CRE stainless steel weldments have also resulted in G-phase precipitation and spinodal decomposition in the ferrite (Refs. 7–9). However, there has been relatively little research directed toward weldments operating at the somewhat lower temperatures typical of the LWR environment. Therefore, a series of welds were fabricated and aged to study the effects of long-term aging at 343°C, the upper operating temperature limit for LWR piping, on the mechanical properties of such welds. Portions of this work have been reported previously (Refs. 10–14). This report presents all of the results available to date.

¹Research sponsored by the Office of Nuclear Regulatory Research, U.S. Nuclear Regulatory Commission, under Interagency Agreement DOE 1886-N695-3W with the U.S. Department of Energy under contract DE-AC05-96OR22464 with Lockheed Martin Energy Research Corp.

EXPERIMENTAL PROCEDURES

Three multipass shielded-metal arc welds were fabricated; the filler metal composition was adjusted to result in target ferrite contents from 5 to 15%. The lower ferrite volume fractions were obtained by increasing the manganese and nickel levels and lowering the chromium level of the steel. Subsequent measurements with a Ferritescope indicated that the welds contained nominally 4, 8, or 12% ferrite. The base metal for all of the welds was 25-mm-thick (1-in.) 304L stainless steel plate. A V-groove geometry was used, which resulted in the top of the weld being approximately 25 mm wide (1 in.), while the bottom was approximately 13 mm wide (0.5 in.). The weld metal was then deposited in the groove against a 304L backing plate. Each weld was approximately 600 mm (24 in.) long. Portions of each weld were initially aged for 3,000, 10,000, or 20,000 h. After material had been removed for the first part of this study (Refs. 10–13), the remaining portions of the welds were returned to the furnace and the agings continued to obtain longer aging times. Material that had been aged for 3,000 h was given 17,000 h more aging to achieve 20,000 h. Material from the original 10,000- and 20,000-h agings were given an additional 40,000- or 30,000-h aging, respectively, to achieve a total of 50,000-h aging (Ref. 14). All agings were conducted in air at 343°C. These aged welds were then compared to as-welded specimens.

Standard Charpy V-notch (CVN) specimens were machined from both the top and bottom of each piece of weldment. These specimens were notched so that the crack would propagate in the direction of welding (T-L orientation). The CVN specimens were tested over an appropriate range of temperatures to study the ductile-to-brittle transition for each of the various ferrite content-aging time combinations. Testing was conducted on a semiautomated 407-J (300 ft-lb) Charpy machine that used a transfer device to carry the specimen from a cooling/heating chamber and position it on the anvils for testing. Heating was provided by a hot-air gun; cold nitrogen gas was used for cooling. After testing, the measured energy values were fitted with a hyperbolic tangent function to allow transition temperatures and the upper-shelf energy to be determined. A value of 6.8 J (5 ft-lb) was assumed for the lower-shelf energy for the computer curve fits because no testing was conducted at lower-shelf temperatures. This allowed the computer program to fit the limited data in a consistent manner. As a result of this choice, the transition temperatures and shifts should not be regarded as absolute values, but merely

estimates. Nonetheless, the shifts in the data and the trends of the impact energy with aging are clear. The lateral expansion of the broken specimens was also measured and fitted with an assumed value of 0 mm for the lower shelf.

Subsize tensile specimens were machined from the top, middle, and bottom of each weldment. The use of subsize specimens [3.2 mm in diameter by 12.7 mm gage length (0.125 by 0.5 in.)] was necessary to ensure that the gage length contained only weld metal and not the 304L base metal. All testing was conducted at room temperature on a screw-driven machine at a constant crosshead speed of 4×10^{-3} mm/s (0.01 in./min) for an initial strain rate of approximately 3×10^{-4} s⁻¹.

The fracture surfaces of selected CVN specimens were examined in a scanning electron microscope (SEM). Some fractured CVN specimens were sectioned perpendicular to the fracture surface, metallographically polished, etched, and examined. For examination in the transmission electron microscope (TEM), 3-mm-diam disks were cut from the top and the middle portions of 12% ferrite material in the as-welded condition and after aging for 20,000 h at 343°C. Philips EM430T (300-kV) and EM400T/FEG (100-kV) electron microscopes equipped with EDAX 9100 energy-dispersive X-ray (EDS) and GATAN 607 electron-energy-loss spectrometers (EELS) were used for analytical electron microscopy examination.

The Oak Ridge National Laboratory atom probe, equipped with an energy-compensated time-of-flight spectrometer (Ref. 15), was used to study the fine-scale decomposition in the ferrite after aging for 20,000 h. For the atom probe field-ion microscopy (APFIM) analysis, specimens cut from the uppermost portions of the weld were electropolished following standard procedures (Ref. 16). Since only a small volume fraction of ferrite was present, all APFIM specimens were previewed in the TEM. If no ferrite was present near the apex of the specimen, the needles were either pulse-polished or repolished and then reexamined in the TEM. This procedure proved to be tedious and, for the most part, unsuccessful. To improve the success rate for obtaining ferrite at the specimen apex, a GATAN model 645 precision ion-milling system was used to ion mill the specimen. This method allows more control over the material removal process; as little as 20 nm may be selectively removed from the tip. More details concerning this procedure are discussed elsewhere (Ref. 17). For the atom probe

analysis, specimens were cooled to either 50 or 60 K and a pulse fraction of 20% was used during the data acquisition.

Atom probe composition profiles through the ferrite that contained more than 10,000 ions were analyzed with a variety of statistical techniques, including chi-square frequency distribution tests, autocorrelation functions, Johnson and Klotz Markov chain analysis (Ref. 18), the Hetherington and Miller mean separation method (Ref. 19), and the sample distribution analysis method developed by the Oxford University atom probe group (Refs. 20 and 21).

One type of statistical technique is based on comparing the frequency histograms of the observed chromium compositions with the histogram expected from a random solid solution with the same mean composition. An alloy that has undergone decomposition should possess a broader histogram, with a bimodal distribution developing at the later stages of phase separation. The standard chi-square test essentially tests whether the observed distribution differs from the binomial distribution associated with a random solid solution. The sample distribution analysis attempts to quantify the extent of phase separation by calculating the compositional range ($2P_a$) of the observed distribution (Refs. 19 and 20).

To construct the frequency histograms, the ion-by-ion data must be divided into blocks of atoms and the local composition of each block calculated. The block size must be chosen with care because if the block size is too small, the histogram is too imprecise, and if the block size is too large, compositional averaging, or aliasing occurs. A more detailed discussion of the effects of block size on the quantification of atom probe data may be found elsewhere (Ref. 22). The atom probe data were analyzed with a variety of block sizes. A fixed block size of 50 ions was used for the histogram analyses presented here; in general this block size also resulted in the lowest statistical errors.

Autocorrelation techniques can also be used to detect phase separation. In this method the data are again divided into blocks and their compositions determined. Then pairs of blocks in the composition profile a certain distance or lag, k , apart are then considered and the autocorrelation function, r_k , for each lag is derived. If both blocks have a positive deviation from the mean composition, or if both blocks have a negative deviation from the mean composition, then a positive correlation will be found. The optimum lag to consider to detect

clustering or phase separation is $k = 1$ (i.e., adjacent blocks in the composition profile). Larger lags may also be considered to evaluate a characteristic distance in a microstructure, such as a periodicity or interparticle spacing.

Another method of analyzing the atom probe ion-by-ion data is to use Markov chain analysis to test for clustering of solute atoms. The Johnson and Klotz method determines an ordering parameter θ from the number of AA, AB and BB pairs of atoms in the data chain and compares the results with that expected from a random solid solution (Ref. 18). Alternatively, the Hetherington-Miller mean separation method may be used to compare the variance of the distances between chromium atoms with that expected from a random distribution (Ref. 19). Both these techniques have been shown to be effective in detecting clustering (Ref. 22), the Johnson and Klotz method being more suited to higher-concentration systems and the mean separation method to dilute solid solutions.

RESULTS

The chemical analyses for each of the welds are shown in Table 1. In each case, there are only slight differences between the composition at the top of the weld and that at the bottom. Typical microstructures from each of the three welds as shown by optical metallography are

Table 1. Chemical composition of the three type 308 stainless steel weld materials (4, 8, and 12% ferrite content)

Nominal ferrite content (%)	Position in weld	Element (wt %)							
		Cr	Ni	Mn	Mo	C	Si	S	P
4	Top	18.7	8.9	2.0	0.22	0.053	0.45	0.016	0.021
	Bottom	19.2	9.7	1.95	0.24	0.056	0.47	0.017	0.029
8	Top	20.5	8.9	1.82	0.24	0.054	0.45	0.013	0.028
	Bottom	19.8	8.6	1.92	0.20	0.053	0.48	0.016	0.025
12	Top	20.8	8.3	1.27	0.20	0.052	0.62	0.012	0.025
	Bottom	20.6	7.8	1.40	0.21	0.052	0.74	0.023	0.028

presented in Figure 1. The microstructure consisted of an austenite matrix with interconnected ferrite regions. As the ferrite content increases, the ferrite regions become larger and more connected. Neither optical metallography nor SEM examination indicated any noticeable changes in the austenite or the ferrite as a function of aging time.

Mechanical Properties

The average values of the room-temperature yield and ultimate tensile strengths for specimens taken from the top, middle, and bottom of the welds are shown in Figure 2. The data indicate that aging does not have a significant effect on any of the strength properties. The bottom of the weld tended to have a slightly higher yield strength while the uniform elongation showed a noticeable decrease for the 12% ferrite material, although it was still high. The yield strength of the as-welded material is inversely proportional to the ferrite content, but this is probably due to scatter as this trend is not consistent with aging. The yield

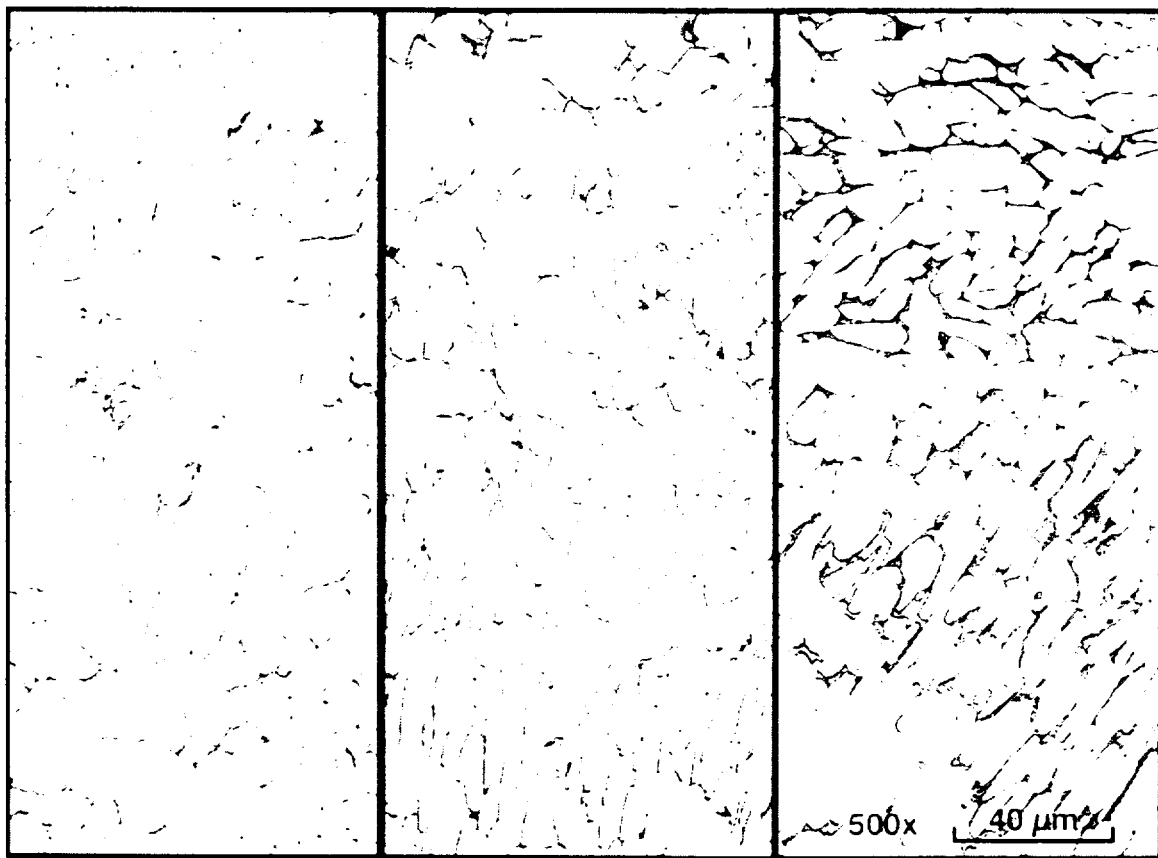


Figure 1. Typical microstructures of the three weld metals. Left, 4% ferrite; middle, 8% ferrite; right 12% ferrite.

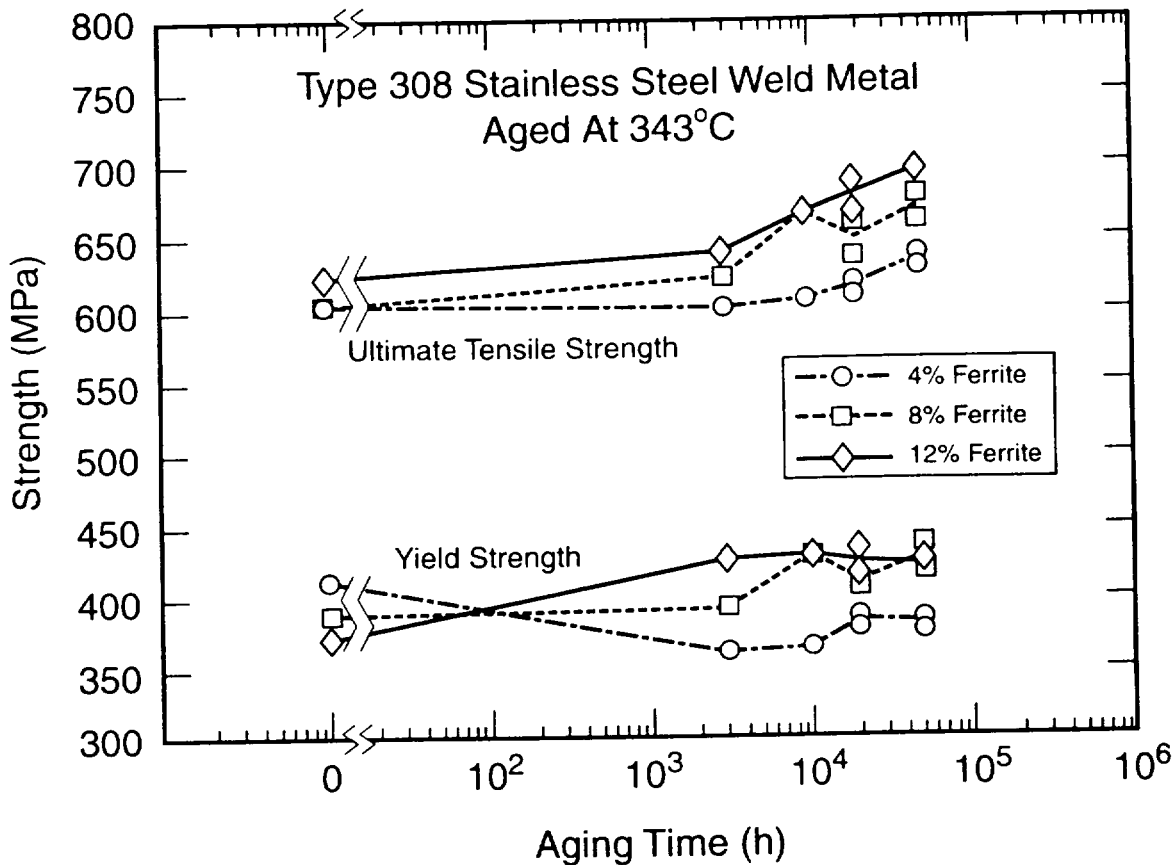


Figure 2. Average yield and ultimate tensile strengths for type 308 stainless steel weld materials aged at 343°C.

strength of the higher ferrite content welds (8 and 12%) increases slightly with increasing aging time, but shows little change beyond the first 3,000 h of aging. The ultimate tensile strength for the higher ferrite welds shows a small continuing increase (about 10% maximum) with increasing aging time to 50,000 h. However, all these effects are relatively small.

The results in Figure 2 also show that aging in two steps rather than a single step has no effect on the tensile properties; the data from the original 20,000-h aging are very similar to new data from material aged 3,000 h plus 17,000 h. Similarly, the results from material aged for 10,000 h plus 40,000 h match well with results from material aged for 20,000 h plus 30,000 h.

The Charpy results show a more pronounced effect and indicate that the aging has a much more significant effect on the dynamic fracture behavior than on the quasi-static tensile

properties. The computer curve fits for the three different ferrite contents are shown in Figures 3, 4, and 5. Table 2 lists the transition temperatures and upper-shelf energy levels.

The transition temperature for each of the groups has been evaluated at 40.7 J (30 ft-lb), 67.8 J (50 ft-lb), and at an energy level midway between the upper- and lower-shelf energy levels ($T_{40.7}$, $T_{67.8}$, and T_0 , respectively). Data from both the top and the bottom of the welds have been combined for the Charpy curve fits because the chemical analysis, tensile tests, and the Charpy tests themselves indicate that there is little difference between the tops and bottoms of these welds. The results show a significant increase in the transition temperature with aging (see Figure 6). Additionally, the upper-shelf energy level decreases with increasing aging time (Figure 6). These effects are more pronounced as the ferrite content increases. Furthermore, the embrittlement continues to increase with increasing aging time, as indicated by higher transition temperatures and lower upper-shelf energy levels. A similar shift was observed in the lateral-expansion measurements, with the 0.89-mm (0.035-in.) transition

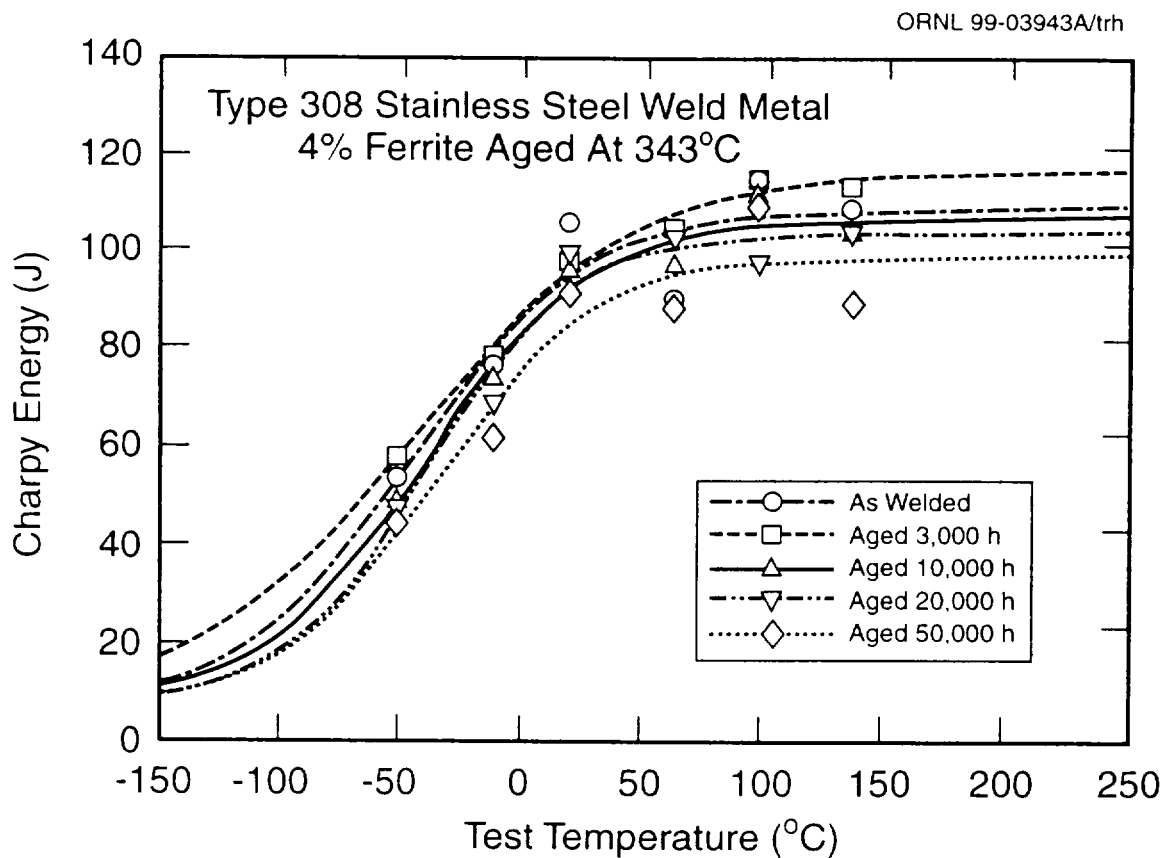


Figure 3. Effect of aging at 343°C on Charpy impact transition curves for type 308 stainless steel weld materials, 4% ferrite.

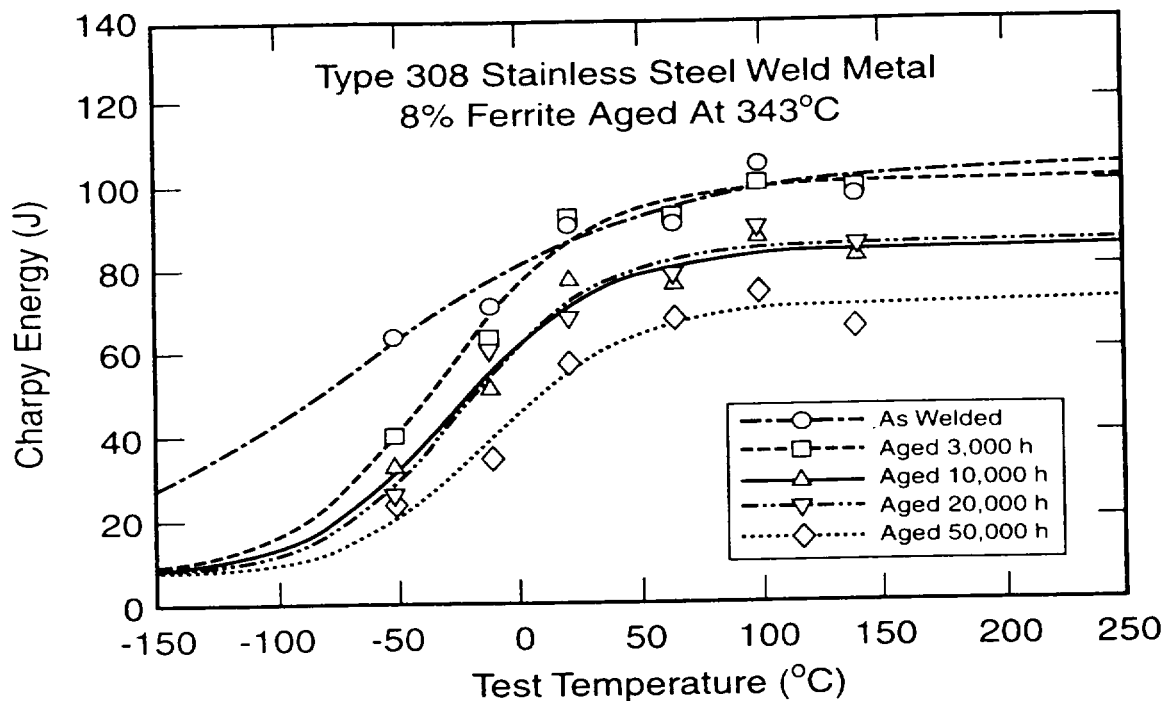


Figure 4. Effect of aging at 343°C on Charpy impact transition curves for type 308 stainless steel weld materials, 8% ferrite.

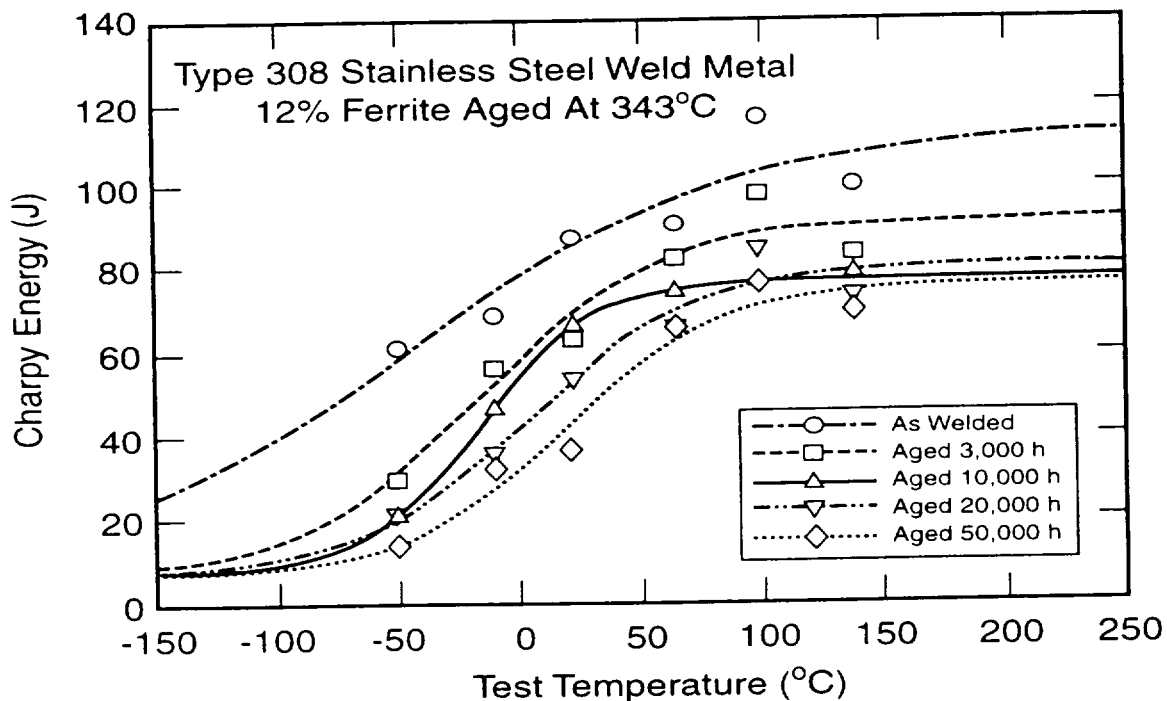


Figure 5. Effect of aging at 343°C on Charpy impact transition curves for type 308 stainless steel weld materials, 12% ferrite.

Table 2. Charpy impact properties for the three type 308 stainless steel weld materials (4, 8, and 12% ferrite content)

Ferrite (%)	Aging time (h)	Transition temperatures (°C)					Upper shelf	
		T ₀ ^a	T _{40.7} ^b	T _{67.8} ^c	T _{LE} ^d	T _{0.89} ^e	Energy (J)	Lateral expansion (mm)
4	AR	-44	-68	-29	-39	-51	108	2.10
	3	-43	-80	-32	-48	-77	116	2.30
	10	-38	-61	-22	-35	-48	107	2.15
	20	-37	-56	-21	-37	-53	103	2.18
	50	-34	-52	-11	-8	-38	98	2.50
8	AR	-66	-104	-35	-70	-83	104	2.00
	3	-30	-47	-11	-39	-39	100	1.80
	10	-26	-33	14	-37	-29	84	1.60
	20	-23	-31	13	-25	-18	85	1.66
	50	-11	-8	75	-7	-10	71	1.85
12	AR	-44	-96	-25	-23	-41	114	2.28
	3	-15	-30	20	-14	-7	91	1.66
	10	-17	-19	29	-9	-2	77	1.64
	20	2	-3	59	9	14	80	1.70
	50	18	17	84	14	20	75	1.65

^aTransition temperature at an energy level between upper- and lower-shelf energy levels.
^bTransition temperature at an energy level of 40.7 J (30 ft-lb).
^cTransition temperature at an energy level of 67.8 J (50-ft-lb).
^dTransition temperature at a lateral expansion level midway between upper- and lower-shelf expansion values.
^eTransition temperature at a lateral expansion value of 0.89 mm (0.035 in.).

temperature increasing and the upper shelf decreasing (except for the 4% ferrite weld) with increasing aging time (see Figure 7). These effects are more pronounced as the ferrite content increases.

Microstructural Observations

The microstructure is shown in greater detail in TEM micrographs of the 12% ferrite material in Figures 8 and 9, which show the austenite matrix and the ferrite islands. Manganese silicides, as identified by EDS analysis and indicated in Figures 8 and 9, were present throughout the

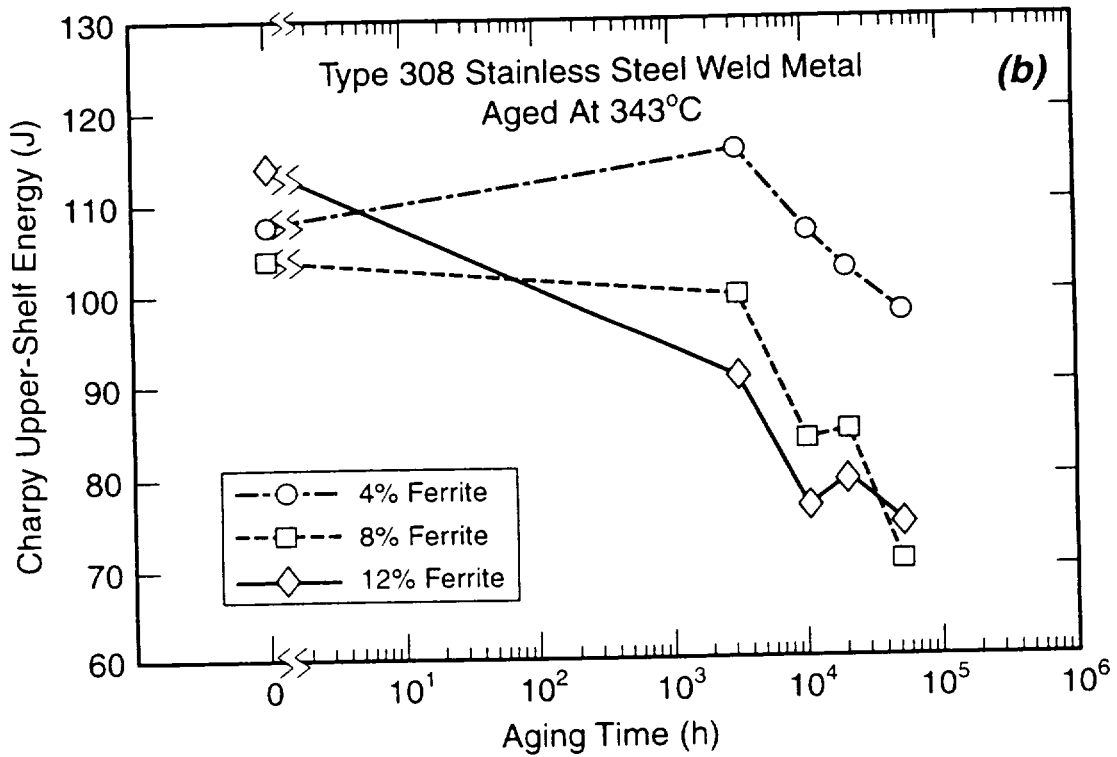
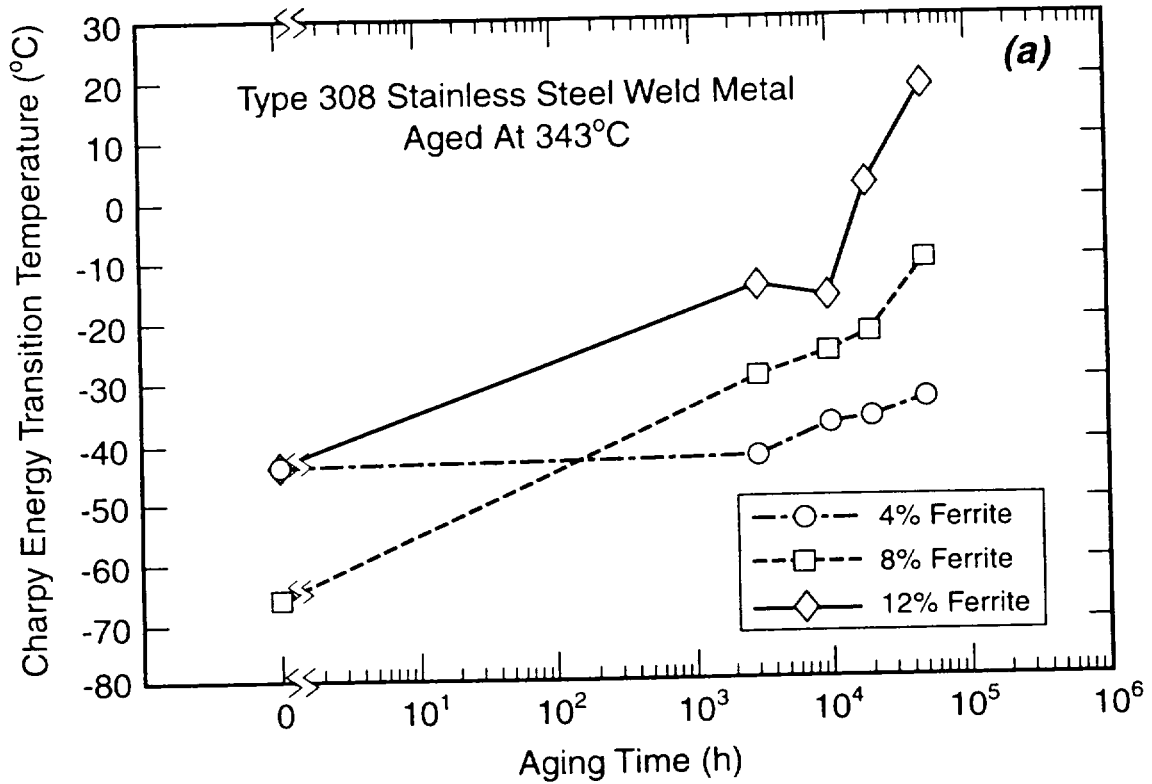


Figure 6. Effects of aging at 343°C on the impact properties of type 308 stainless steel weld metal. (a) Transition temperature versus aging time, and (b) upper-shelf energy versus aging time.

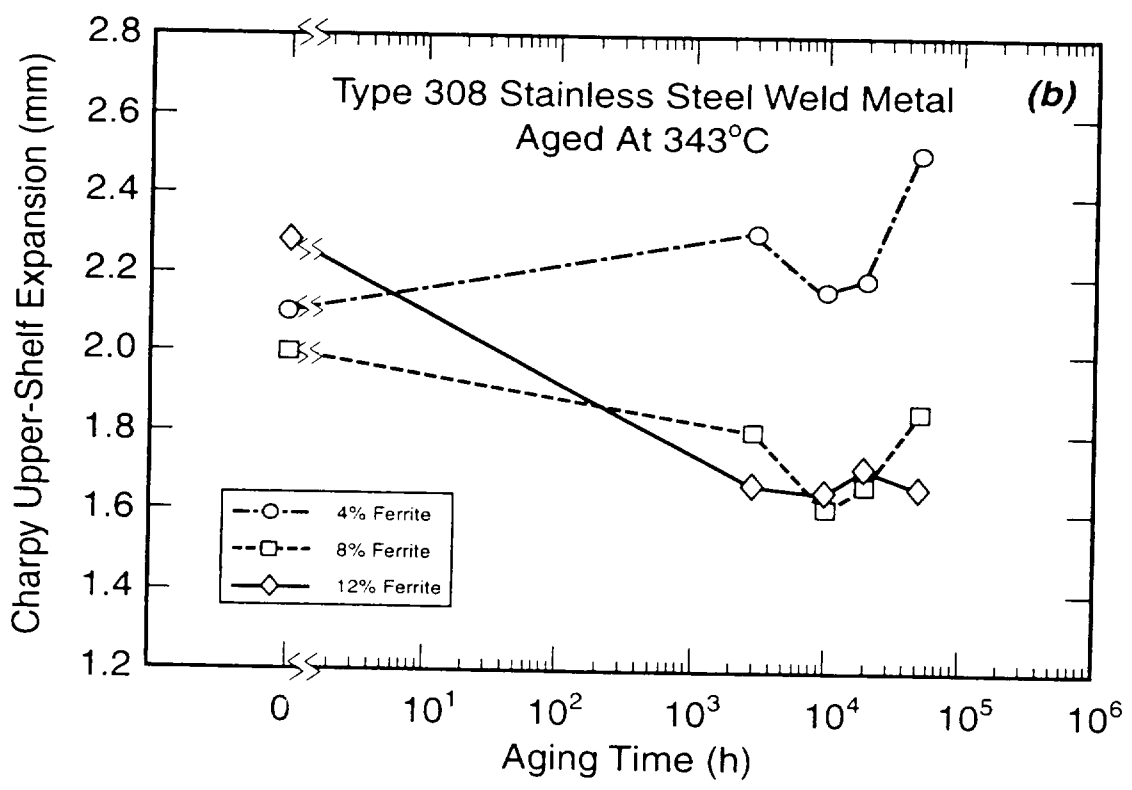
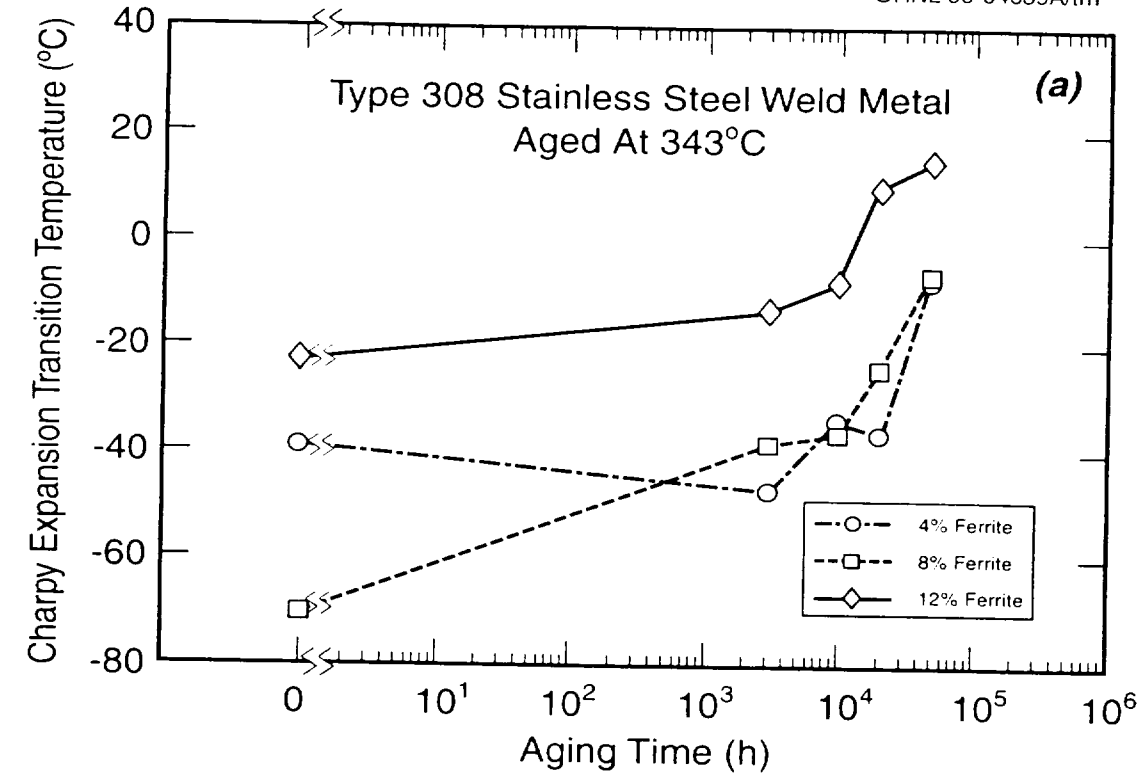


Figure 7. Effects of aging at 343°C on the lateral expansion properties of type 308 stainless steel weld metal. (a) Transition temperature as measured at a lateral expansion of 0.89 mm (0.035 in.), and (b) lateral expansion upper-shelf value.

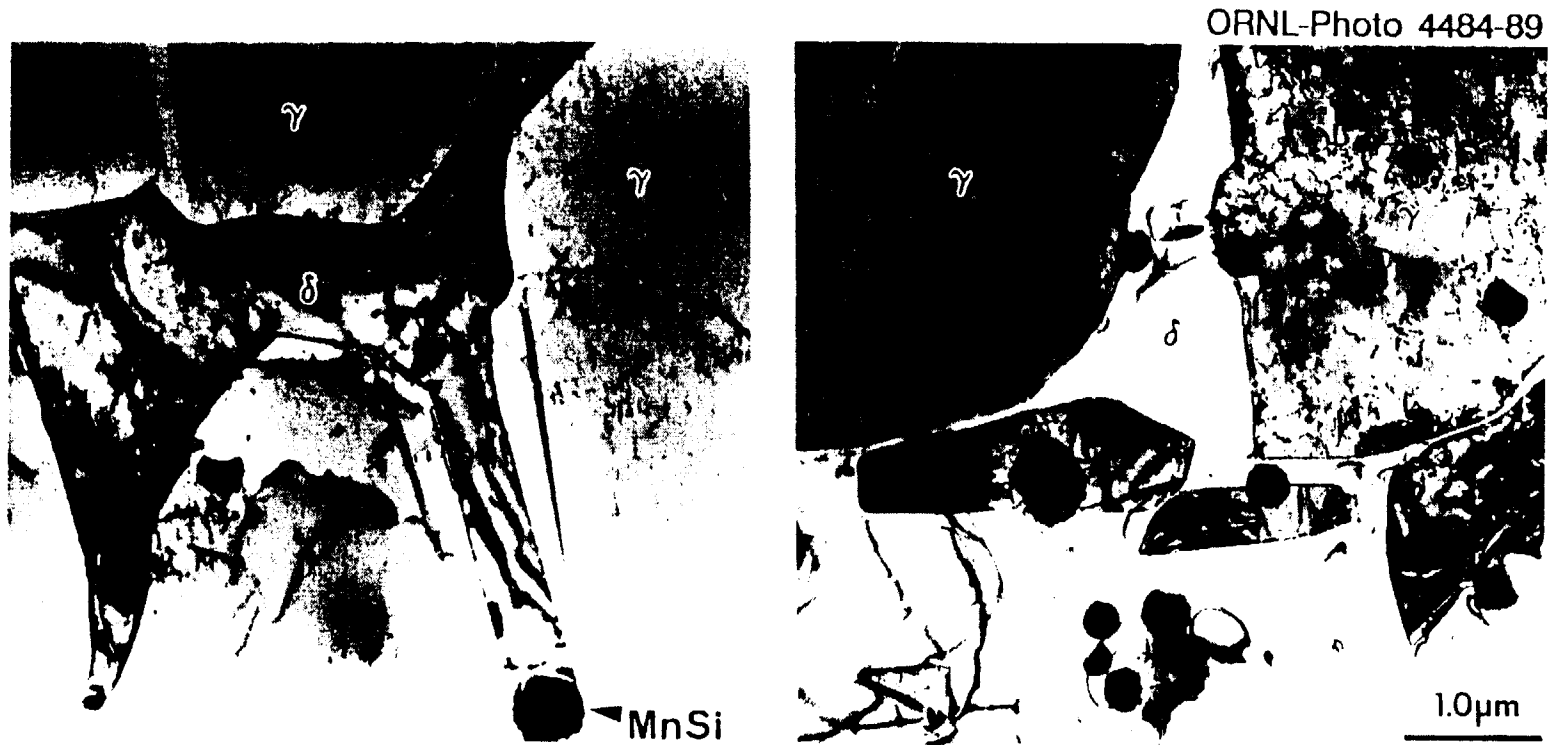


Figure 8. Microstructure from the top of the type 308 stainless steel weld, 12% ferrite material, aged at 343°C for 20,000 h. Note the absence of carbide particles along the ferrite-austenite interfaces and the spherical MnSi particles.



ORNL-Photo 4476-89



Figure 9. Microstructure from the middle of the type 308 stainless steel weld, 12% ferrite, aged at 343°C for 20,000 h. Note the carbides along many of the ferrite-austenite interfaces and the spherical MnSi particles.

weld. $M_{23}C_6$ carbides with a cube-on-cube orientation relationship with the austenite were present at the ferrite/austenite interface (Figure 10). The composition of the $M_{23}C_6$ carbides formed in these alloys is similar to those observed in CF8-type stainless steels. (Refs. 3–5). The heavy-atom component of the composition (atomic percent) of the carbides was determined from EDS analysis to be 75.2Cr-20.7Fe-2.11Ni-0.92Si-1.06Mn. Carbon could not be detected with the EDS system used, but was shown to be present by EELS.

The carbide distribution varied through the weld as shown in Figures 8 and 9. Near the top of the weld (Figure 8), few carbides were observed at the ferrite-austenite interfaces, whereas in the middle portions of the weld, many carbides were observed (Figure 9). SEM examination of metallographic samples confirmed this distribution of the carbides for all of the welds. This distribution suggested that these carbides were formed during the welding process when prior weld beads were reheated by the application of subsequent passes. No significant change in the carbide distribution was observed as a function of aging treatment.

An EDS composition profile across a ferrite arm is shown in Figure 11(a). The austenite is enriched in nickel and depleted in chromium as compared to the ferrite. The chromium levels obtained by EDS analysis are slightly overestimated (by 1 to 2%) because of the fluorescence of chromium by iron K_{α} X-rays. The APFIM composition profile across the austenite/ferrite interface shown in Figure 11(b) confirms the nature of chromium and nickel partitioning between the two phases. Because the atom probe samples the specimen on an ion-by-ion basis, any segregation to the austenite/ferrite interface can be readily detected. The character plots in Figure 12 indicate both carbon and phosphorous segregation at the interface. The compositions of one austenite and three different ferrite regions as determined using APFIM analysis are summarized in Table 3.

The type 308 weld material investigated in this study is richer in manganese and lower in silicon than the CF8-based alloys studied previously after aging in this temperature regime (Refs. 3–5). Manganese silicides are present throughout the weld microstructure, and several can be seen in Figures 8 and 9. It is therefore expected that the manganese silicides reduce the amount of silicon available in the ferrite to form the complex G-phase silicide. In CF8-type materials, the G-phase contains nickel, iron, molybdenum, chromium, carbon, and silicon (Refs. 3–5).

ORNL-Photo 4479-89

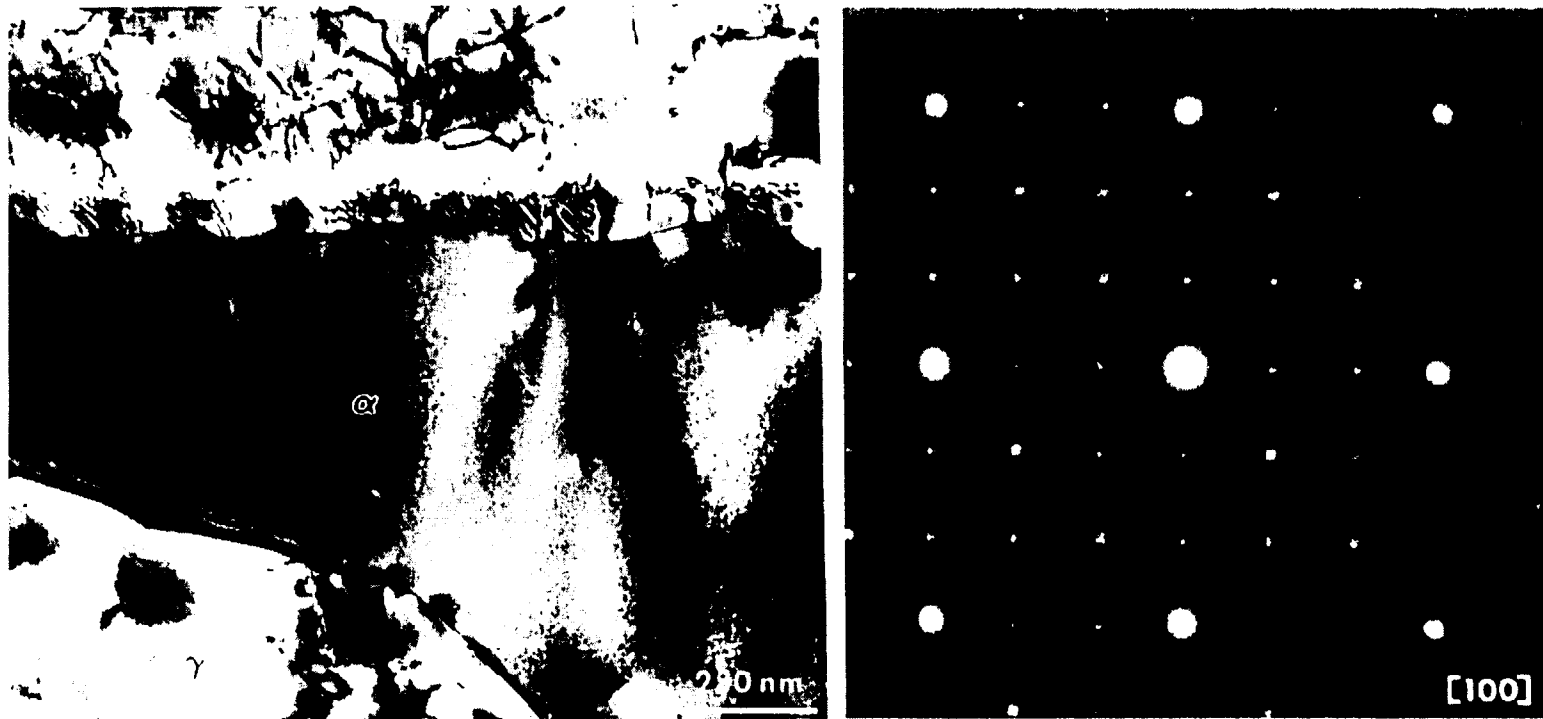


Figure 10. $M_{23}C_6$ carbides at the austenite-ferrite interphase boundaries of the type 308 stainless steel weld, 12% ferrite, aged at 343°C for 20,000 h. Left: view of cuboidal particles; right: diffraction pattern showing cube-on-cube orientation relationship of carbides with austenite matrix.

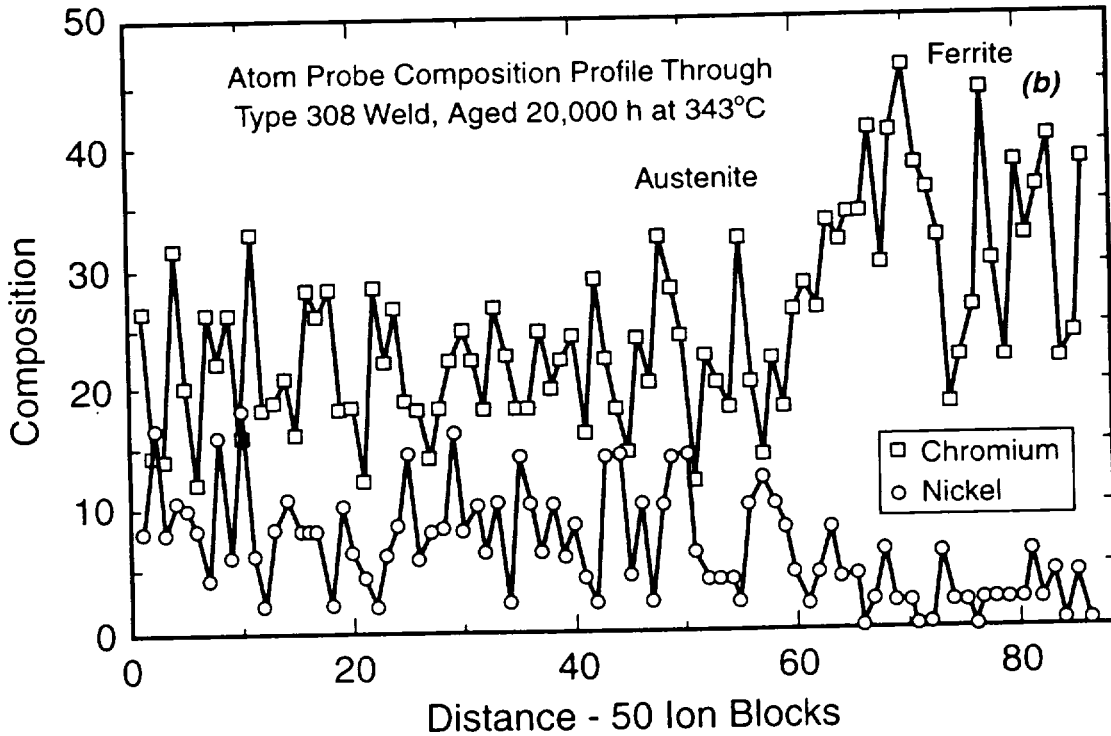
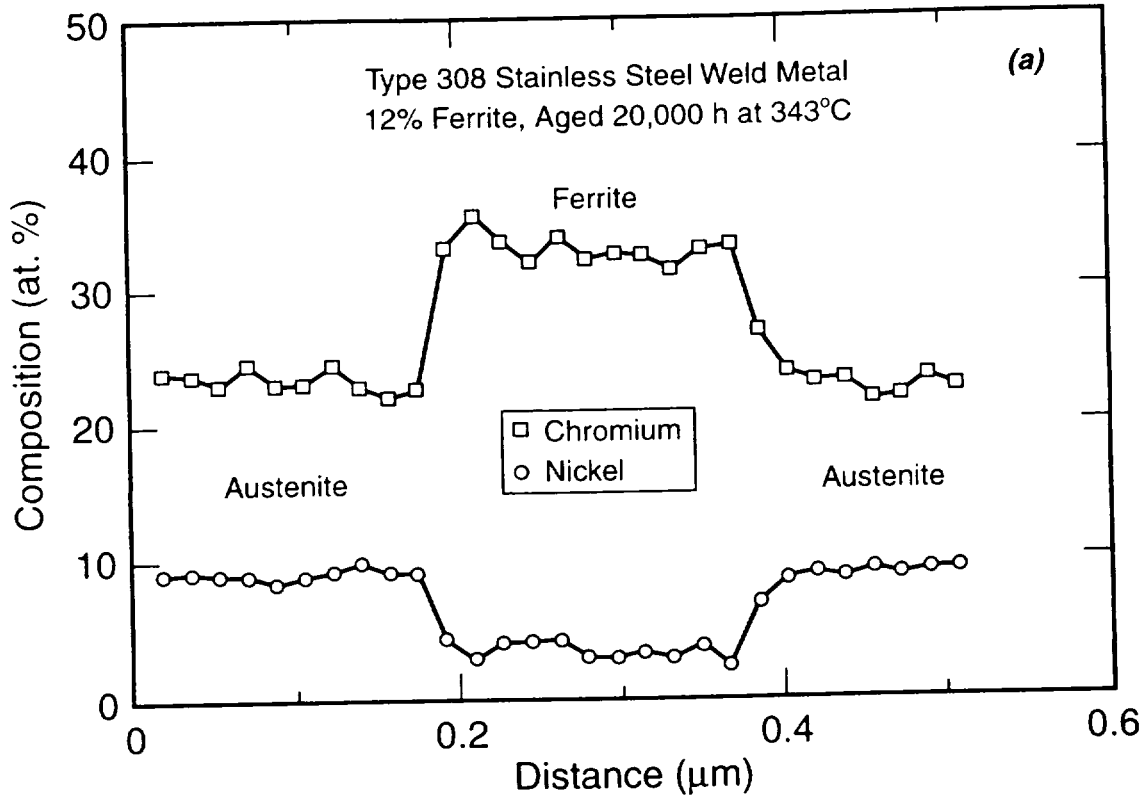


Figure 11. Chromium and nickel composition profiles of the type 308 stainless steel 12% ferrite weld aged at 343°C for 20,000 h. (a) Obtained from EDS analysis, and (b) obtained from atom probe.

Dark-field imaging techniques revealed the presence of fine (4- to 6-nm) G-phase precipitates on, or close to, dislocations in the ferrite. The dislocations associated with the G-phase precipitates often appear to be pinned, as shown in Figure 13. This behavior has been previously observed in CF8-type materials (Refs. 3–5). The dark-field image in Figure 13(b) was recorded with the strongest G-phase reflection, $g = (333)_G$. As reported in other studies (Refs. 3–5), the G-phase precipitates have a cube-on-cube orientation relationship with the

Table 3. Compositions of austenite and ferrite aged for 20,000 h at 343°C determined by atom probe field-ion microscopy

Phase	Composition (wt %)					
	Cr	Ni	Mn	Si	Mo	Fe
Aged ferrite 1	29.9	3.81	0.70	1.42	0.08	Bal.
Aged ferrite 2	31.3	2.79	0.67	0.67	0.20	Bal.
Aged ferrite 3	30.29	3.43	0.83	0.83	0.26	Bal.
Aged austenite	21.0	8.48	0.74	0.74	0.14	Bal.

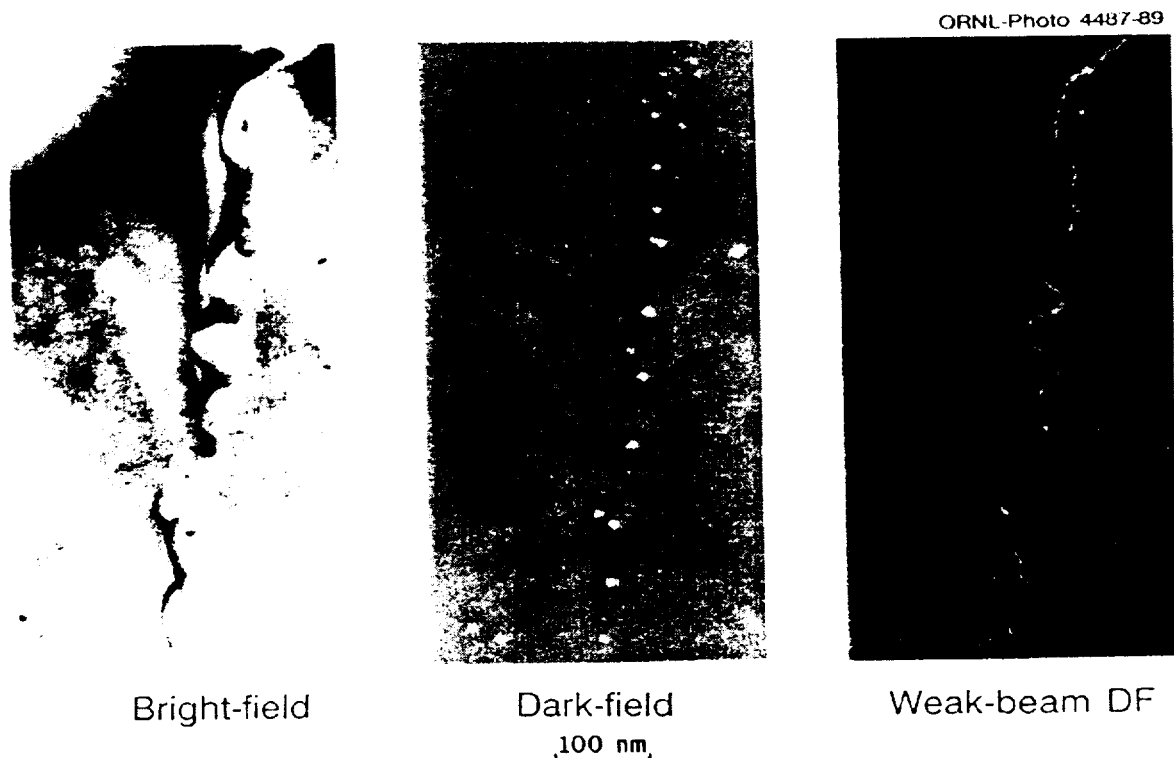


Figure 13. G-phase precipitation in 12% ferrite weld after 20,000 h at 343°C. (a) Bright-field micrograph, (b) $(333)_G$ dark-field micrograph, and (c) weak-beam micrograph showing dislocation.

ferrite matrix (Figure 14). Fine G-phase precipitates up to 2.5 nm in diameter were also observed distributed throughout the ferrite matrix, as shown in the background of Figure 15.

The aged ferrite showed a mottled appearance in bright-field conditions (Figure 16). This mottled appearance is frequently associated with spinodal decomposition. Faint contrast modulations with a periodicity of approximately 6.3 nm were observed in the ferrite under carefully controlled phase-contrast imaging conditions, which distinguish any oxide films from the decomposition products (Refs. 3–5). In order to study the ferrite decomposition further, APFIM analysis was performed.

Field-ion images of the ferrite in the aged material showed no obvious decomposition into iron-rich and chromium-rich regions, but ultrafine brightly imaging G-phase precipitates of low number density were observed (Figure 17). Atom probe composition profiles through both the aged and unaged ferrite are shown in Figure 18. The aged specimens exhibit larger chromium composition deviations than the unaged specimens.

To better quantify the nature of the decomposition in the ferrite, three composition profiles, each with greater than 10,000 ions, were subjected to a variety of statistical analyses. The results of these statistical techniques, which were performed to test whether phase separation into iron-rich and chromium-enriched phases had occurred, are summarized in Table 4, together with the appropriate standard deviations. The statistical significance of these techniques is also shown in Table 4; the figures quoted are the number of standard errors by which the measurement differs from that expected from a random solid solution. Numbers greater than 2 or 3 are to be considered statistically different from a random solution. Chromium composition profiles from unaged ferrite and aged austenite were also subjected to these statistical techniques, and the results are included in Table 4 for comparison. The results indicate that the aged ferrite had phase separated, whereas most of the statistical tests indicated that the chromium in the unaged ferrite and the austenite was randomly distributed. Autocorrelation function analysis of the aged ferrite exhibited a distinct maximum, indicating a periodicity in the microstructure of approximately 6.6 nm. This periodicity is related to the characteristic wavelength of the phase decomposition. The difference in the amplitude of the

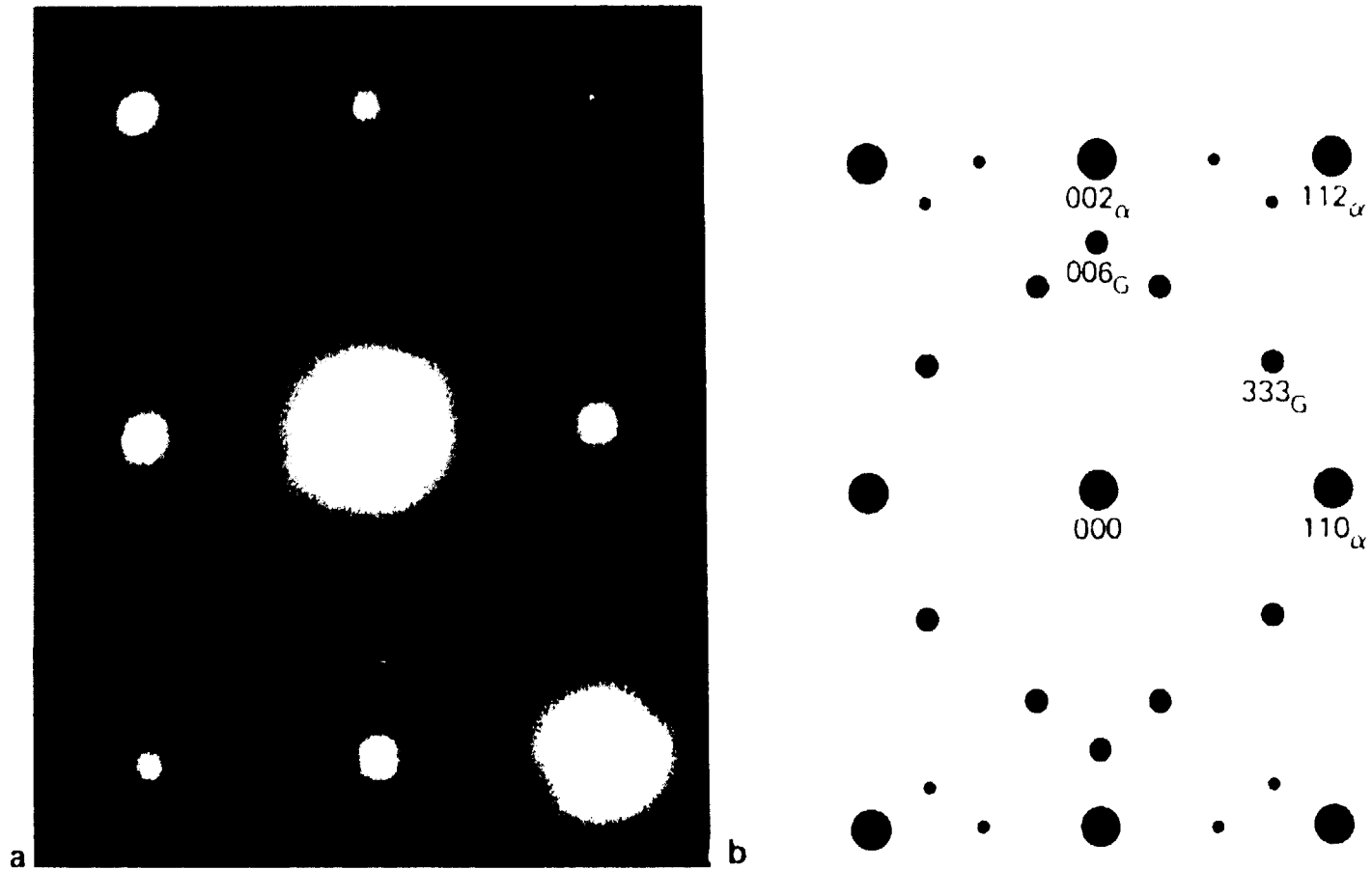


Figure 14. G-phase precipitation in 12% ferrite weld after 20,000 h at 343°C. (a) Diffraction pattern from a (110) zone axis in the ferrite showing G-phase reflections, and (b) superimposed G-phase and ferrite (110) simulated diffraction patterns. Only the most intense reflections are shown.

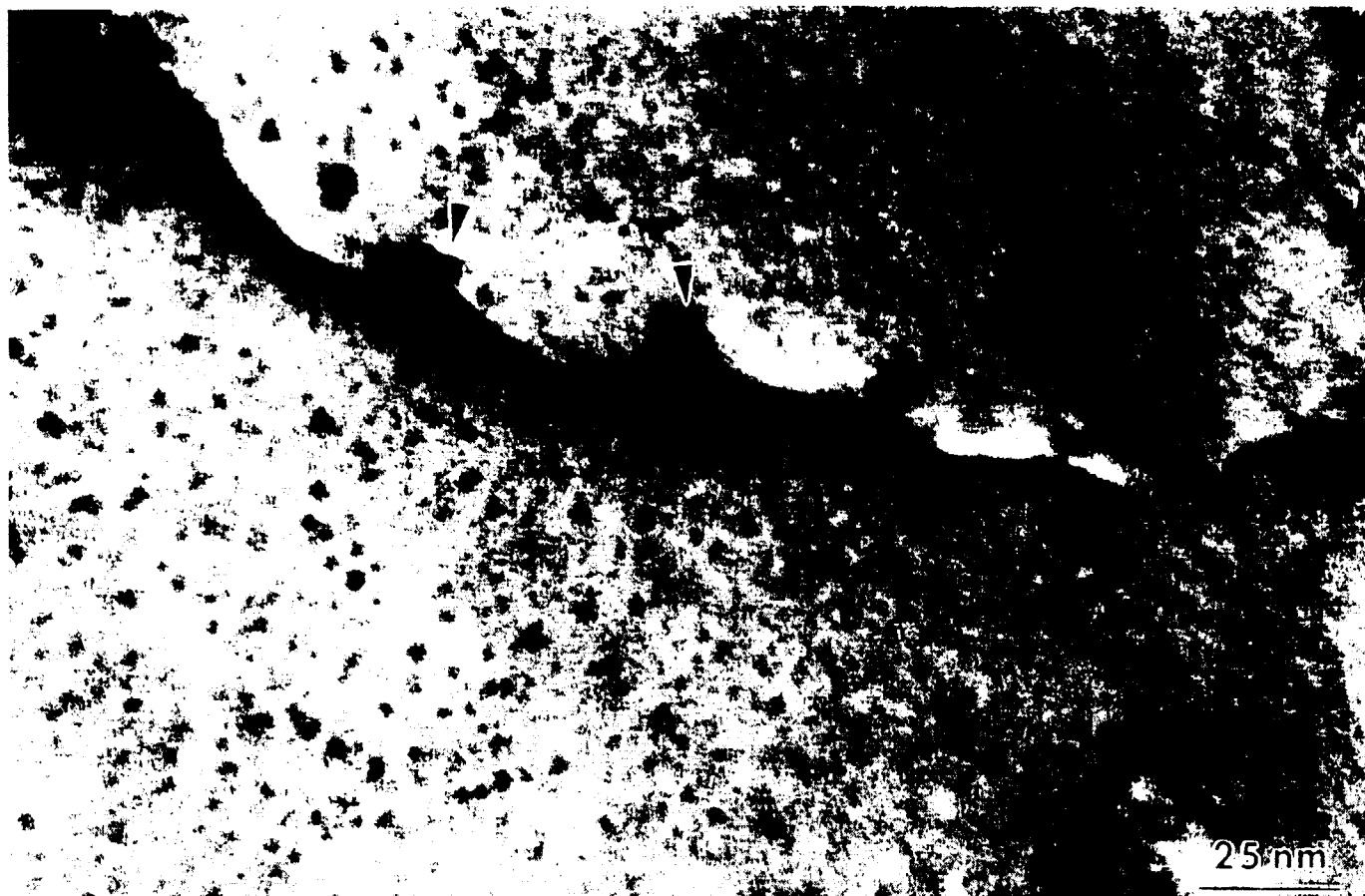


Figure 15. Bright-field micrograph of G-phase precipitation in 12% ferrite weld after 20,000 h at 343°C. The arrows indicate large G-phase precipitates associated with dislocations. G-phase precipitates (dark) are also observed in the matrix.

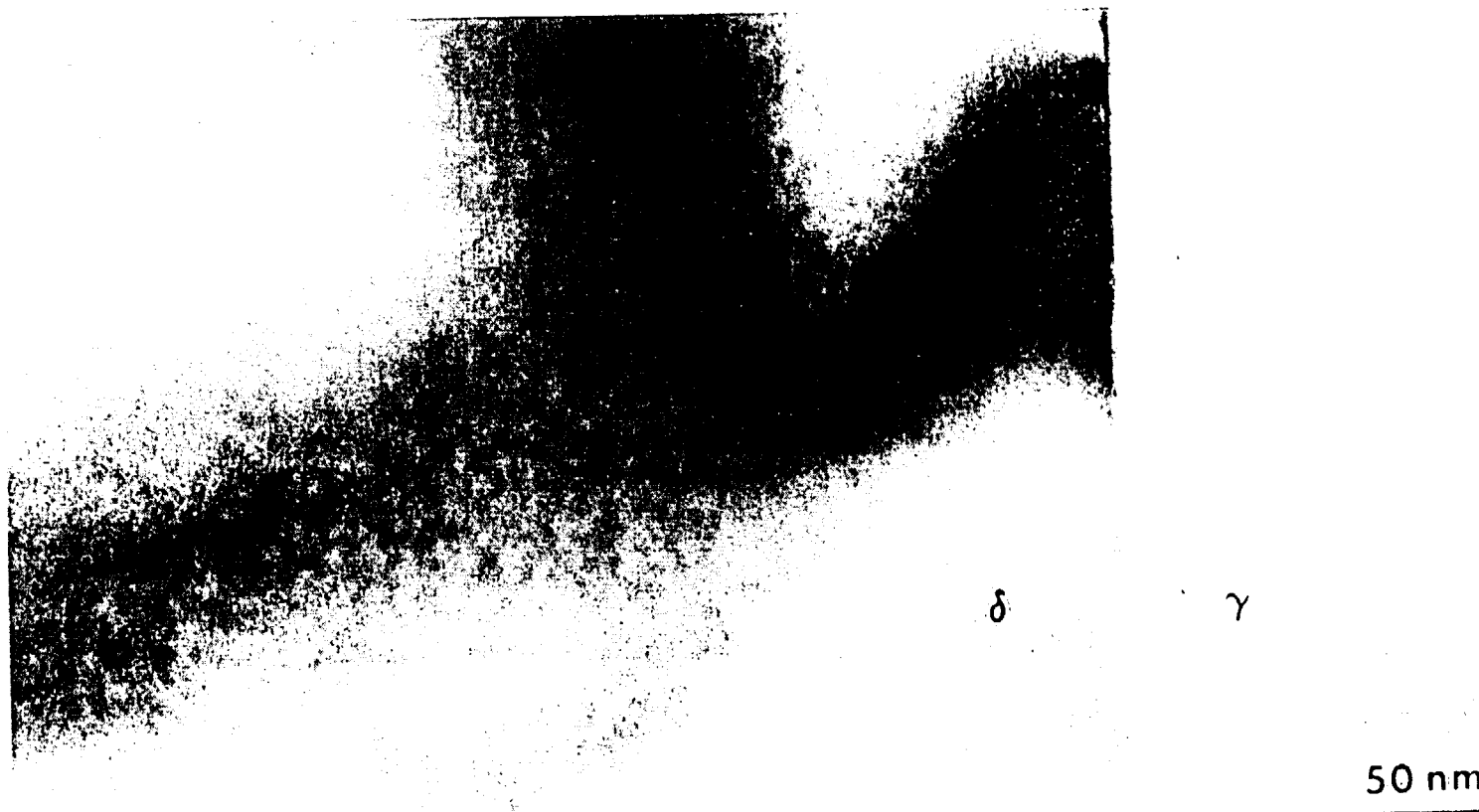


Figure 16. Bright-field micrograph of the ferrite-austenite interphase boundary in the 12% ferrite weld showing the mottled appearance of the ferrite (left) after aging 20,000 h at 343°C. Such a mottled appearance is frequently associated with spinodal decomposition. Note the absence of mottling in the austenite phase (right).

ORNL-Photo 4483-89

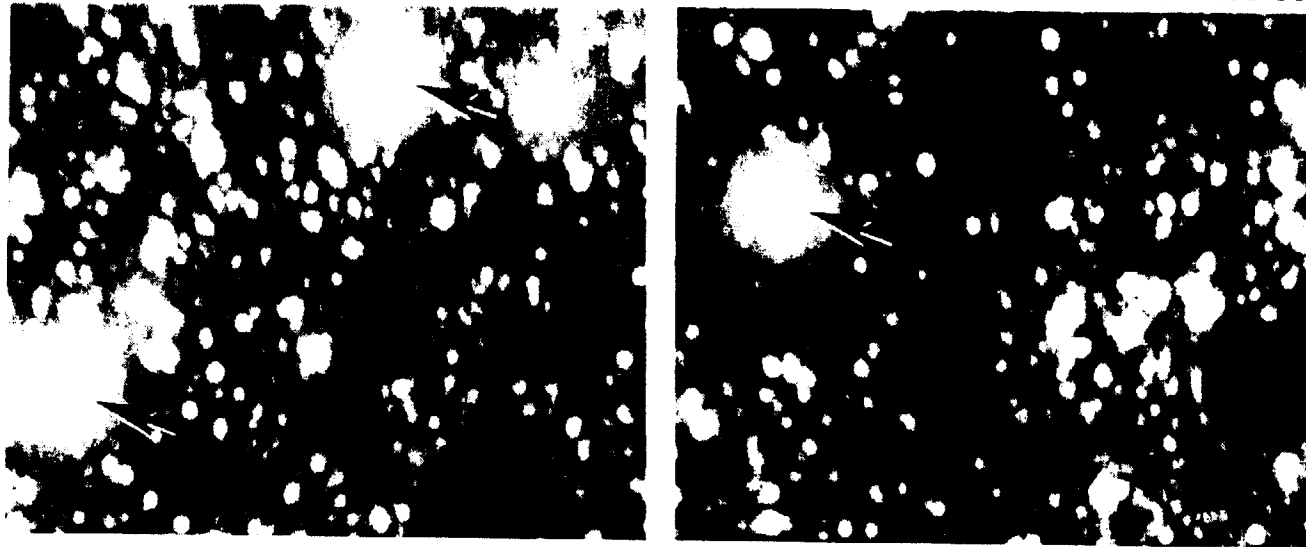


Figure 17. Field ion micrograph of the 12% ferrite weld aged 20,000 h at 343°C, showing brightly imaging ultrafine G-phase precipitates in the ferrite phase.

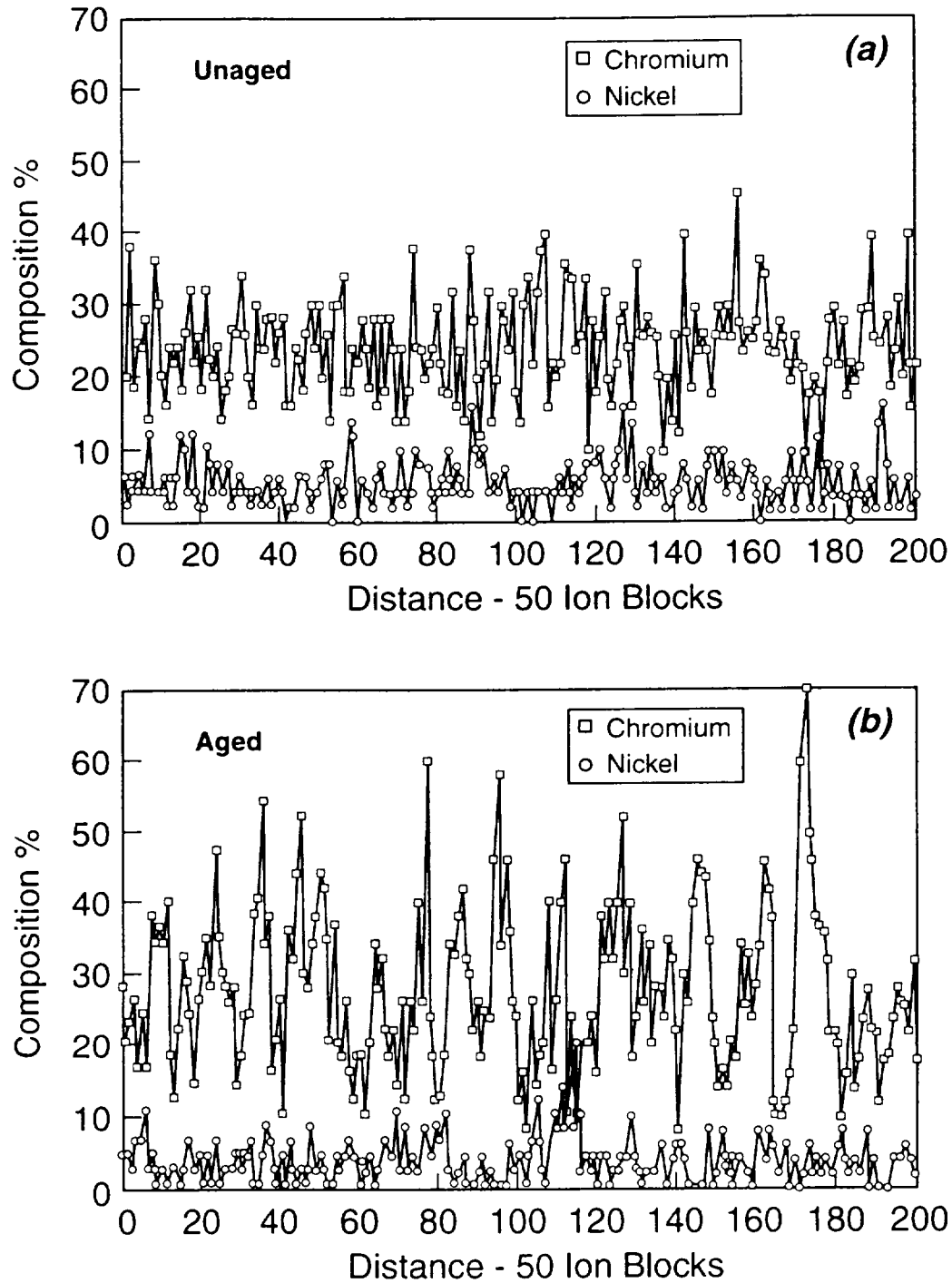


Figure 18. Atom probe chromium composition profiles of the 12% ferrite weld using a 50-ion block size, through the (a) unaged ferrite and the (b) ferrite aged at 343°C for 20,000 h. Phase separation into iron-rich and chromium-enriched regions is evident in (b), showing larger chromium deviations.

Table 4. Statistical analysis of atom probe data (same specimens as Table 3)

Phase	Sample distribution analysis (P_a)	Autocorrelation function (r_1)	J and K ¹⁰ Markov chain		Mean separation significance	Frequency distribution ^a	
			(θ)	Significance		(χ^2)	Degrees of freedom
Unaged ferrite	0.04 ± 0.006	0.04 ± 0.03	1.034	1.72	1.10	22.5	14
Aged ferrite 1	0.05 ± 0.005	0.05 ± 0.02	1.035	2.54	1.93	40.7	17
Aged ferrite 2	0.09 ± 0.006	0.09 ± 0.03	1.131	6.47	4.98	24.0	17
Aged ferrite 3	0.15 ± 0.006	0.15 ± 0.01	1.24	9.69	11.28	26.6	22
Aged austenite	0.03 ± 0.009	-0.03 ± 0.06	0.998	-0.05	-0.58	12.3	12
Number of errors from random distributions							
Unaged ferrite	6	3	1.7	1.1	1.1	R	—
Aged ferrite 1	10	4	2.5	1.9	1.9	NR	—
Aged ferrite 2	15	7	6.5	5.0	5.0	(N)R	—
Aged ferrite 3	25	51	9.7	11.3	11.3	R	—
Aged austenite	3	-0.05	-0.05	-0.06	-0.06	R	—
^a R = random; NR = nonrandom; (N)R = (non)random.							

decomposition ($2P_a$) from 10 to 30% Cr indicates a variation from one ferrite region to another. However, due to the problems of simultaneously sampling both phases, the observed distributions and P_a will probably underestimate the actual composition fluctuations present in the material.

The Johnson and Klotz Markov chain analysis and the Hetherington and Miller mean separation method were applied to the atom probe data to investigate whether the nickel and silicon in solution in the ferrite were randomly distributed or in the form of G-phase precipitates. No clustering of either element was detected. The dislocation density in the ferrite was too low to randomly intercept any heterogeneously precipitated G-phase in the atom probe cylinder of analysis. These observations do not preclude the possibility of a low number density of G-phase precipitates being present as indicated by both the TEM and APFIM observations.

SEM examination of the fracture surfaces revealed that specimens tested on the upper shelf failed by microvoid coalescence, with the fracture surface entirely covered with dimples (Figure 19). As the test temperature decreased, flat areas that appeared to be cleavage were observed. At the lowest temperatures, the percentage of the surface showing microvoids was greatly reduced, and the flat cleavage features dominated (Figure 20).

DISCUSSION

Long-term aging at 343°C can have significant effects on the microstructure and mechanical properties of type 308 weld material. The most significant changes are observed in the ferrite and the Charpy impact properties.

The APFIM results and the contrast modulations in the TEM micrographs indicate that the aged ferrite shows phase separation into the iron-rich α phase and the chromium-enriched α' phase, whereas the unaged ferrite and the aged austenite do not. This phase separation is indicative of spinodal decomposition within a low-temperature miscibility gap (Ref. 23). It

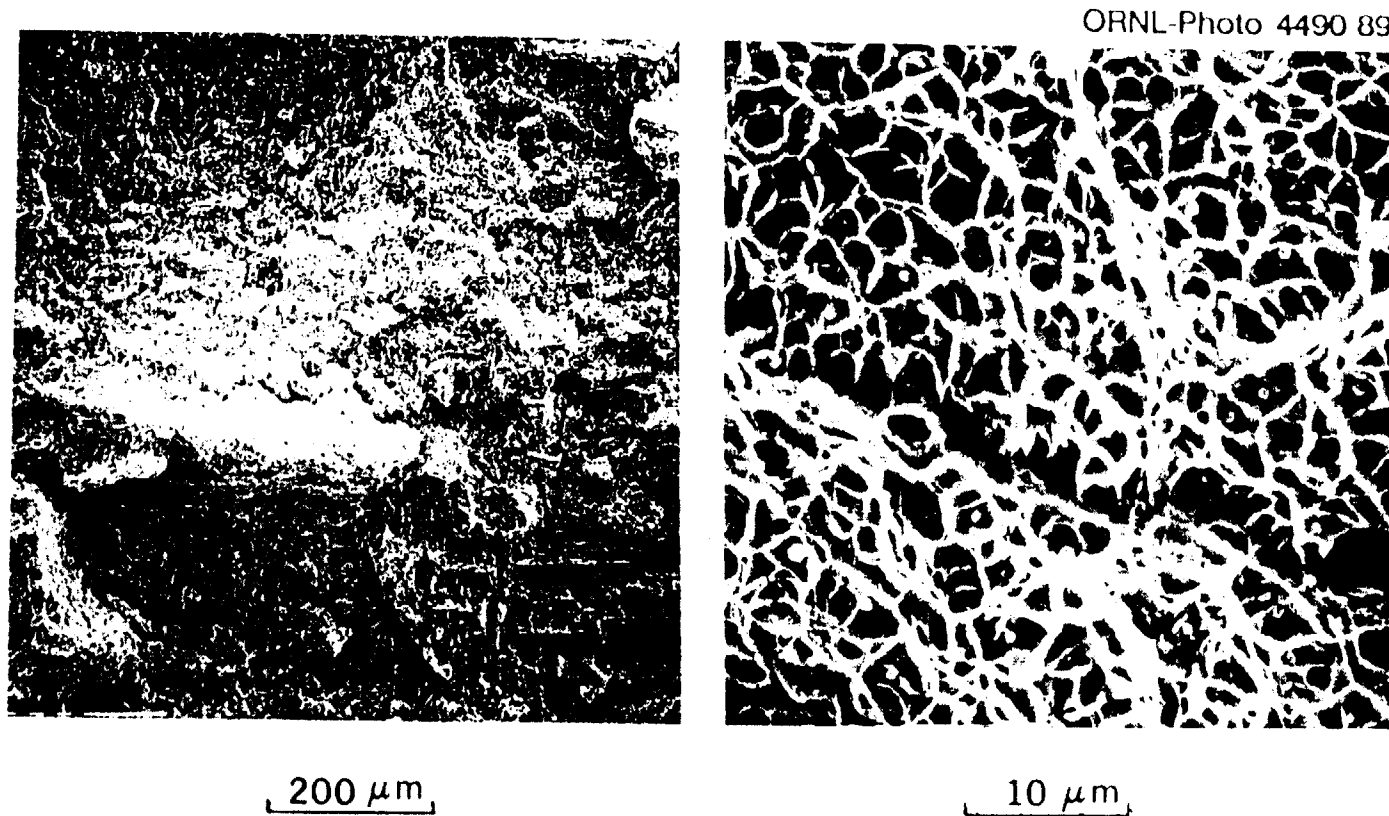


Figure 19. Fractography of type 308 stainless steel weld metal specimen tested on upper shelf. Left: low-magnification view showing rugged fracture surface; right: higher magnification showing ductile microvoid coalescence; 12% ferrite, unaged, tested at 100°C.

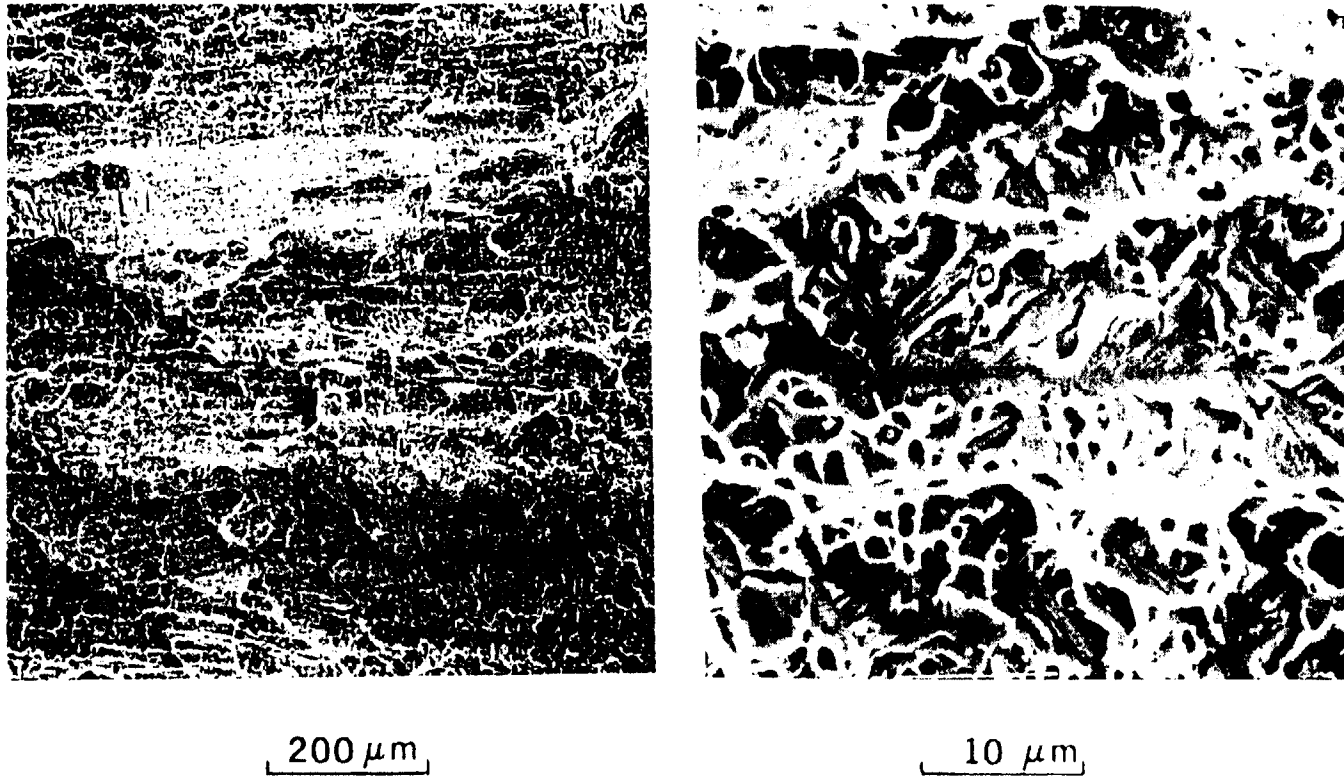


Figure 20. Fractography of type 308 stainless steel weld metal specimen tested in transition regime. Left: low-magnification view showing stepped appearance of fracture surface; right: higher magnification view showing flat regions with cleavage-like appearance. 12% ferrite material, aged at 343°C for 20,000 h, tested at -50°C.

should be emphasized that it is necessary to analyze the APFIM composition profiles by means of a variety of statistical techniques to ensure correct interpretation of the data. The ultrafine scale of the phase decomposition, measured from the contrast modulations in the TEM micrographs and determined from the autocorrelation analysis of the atom probe composition profiles, was consistent with previous investigations of the decomposition in the low-temperature miscibility gap in the Fe-Cr system (Ref. 23). The presence of the iron-rich and chromium-rich regions is in agreement with investigations on CF8 materials that exhibit similar changes in mechanical properties (Refs. 3–5).

The observed G-phase precipitates on dislocations were 5 to 6 nm in diameter, whereas those in the matrix were at most 2.5 nm. In type CF8 steel aged at 300 and 400°C, Miller and Bentley observed G-phase both on dislocations and homogeneously distributed throughout the ferrite (Refs. 3-5). The precipitates on the dislocations were 4 to 5 times larger than those in the matrix. Chopra and Chung also observed both homogeneous and heterogeneous G-phase precipitation in type CF8 alloys aged at 300 to 400°C (Ref. 6). Vitek et al. detected G-phase precipitation on dislocations in type 308 welds aged at 475°C (Refs. 7–9). Sassen et al. applied contingency table analysis to atom probe data but did not detect G phase in type CF3 stainless steel aged at 400°C (Ref. 20).

The ferrite in the type 308 stainless steel material examined in the present study contains less silicon and more manganese than that in the CF8 material examined by Bentley and Miller (Refs. 3–5). The lower levels of silicon readily explain the small volume fraction of G-phase observed in these materials. It should be emphasized that great efforts were made to identify G-phase precipitation. The strongest reflection (333_G) was used to obtain the dark-field images, and was itself quite weak.

The mechanical tests indicate that long-term aging, even at temperatures as low as 343°C, can have a significant effect on the dynamic fracture properties of type 308 stainless steel weld metal, despite little apparent effect on the quasi-static tensile properties. Although the ferrite is present in rather limited amounts (at most 12%), it apparently plays a critical role in the fracture process at high strain rates.

The microhardness of the ferrite and austenite has been studied¹ for the 12% ferrite weld aged up to 20,000 h by using a specially designed nanohardness indenter capable of sampling the very small ferrite regions in the weld structure (Ref. 24). The data indicate that the austenite phase is unaffected by the aging, but the hardness of the ferrite increases considerably, even after only 3,000 h. These increases in hardness in the aged ferrite have also been observed for similar weldments aged at 475 °C (Ref. 9). Despite this increase, the yield and ultimate strengths are largely unaffected, indicating that yielding, plastic flow, and fracture can be accommodated in the austenite under the slow strain rates and low constraint conditions present in the tensile geometry.

The transition from higher-energy to lower-energy fracture as the test temperature is decreased for even the 4% ferrite material in the as-welded condition serves to emphasize the significant effect that even a small amount of ferrite can have on the dynamic fracture process. As Figure 1 shows, the ferrite in the low-ferrite weld is generally dispersed into small, apparently isolated regions, and yet the weld metal displays a ductile-to-brittle transition as the test temperature is decreased. This suggests that the ferrite content would have to be reduced to very low levels or the individual particles would have to be quite small to eliminate this transition. Other work with similar weldments that have an extremely low ferrite content has shown that better impact energies can be obtained at cryogenic temperatures (Ref. 25).

The upper-shelf energy levels for these welds are quite low in the as-welded condition. This is somewhat surprising because fracture occurs by a ductile mode and the tensile results show good strength and high ductility. However, the abundant MnSi particles produced during the weld fabrication provide many sites for nucleation of closely spaced voids, and thus ductile fracture is greatly enhanced. These particles are clearly evident on the fracture surface (see Figures 19 and 20). Reducing the number and size of these MnSi inclusions should result in improvement of the upper-shelf energy.

The Charpy data indicate that there are two effects occurring with aging: the transition temperature increases, and the upper-shelf energy decreases. Also, the magnitude of these effects increases with ferrite content. The increase in transition temperature is believed to be

¹S. G. Druce, unpublished research, ORNL and UKAEA, Harwell, 1988.

the result of easier initiation of cleavage fracture in the ferritic regions of the material, caused by the hardening of the ferrite. Sections taken perpendicular to the fracture surface revealed small microcracks associated with the ferrite near the fracture surface (Figure 21). This suggests that fracture begins in the ferrite phase, probably by a cleavage process, and then continues through the austenite matrix. SEM stereo pairs show that the fracture surfaces of specimens broken in the transition region are extremely rugged and consist of many large flat regions roughly parallel to the macroscopic fracture plane linked by steep slopes approximately perpendicular to the fracture plane. The fracture path appears to preferentially follow the ferrite phase. This observation also explains why the embrittlement increases with the ferrite content because the ferrite becomes larger and more interconnected as the volume fraction increases. The increase in the size of the ferrite regions makes cleavage initiation easier and increases the size of the microcracks, and the greater amount of interconnection of the ferrite as the volume fraction of ferrite increases makes the crack propagation easier as well.

The reason for a decrease in the upper-shelf energy is less apparent, as the fracture process at higher temperatures is ductile, and thus should be controlled by the austenite matrix. There is no change in the microhardness of the austenite with aging,⁷ and no changes in the microstructure within the austenite were observed in this work. Examination of the microstructure near the fracture surface revealed the presence of martensite in the austenite matrix, although the amount of martensite appeared to be independent of the aging conditions. It is possible that the increase in hardness of the ferrite results in the transfer of strain to the austenite matrix, which in turn promotes the formation of martensite, resulting in a decrease in the upper-shelf energy. Prior work with similar material aged at 475°C has suggested that the decrease in upper-shelf energy is due to the G-phase (Ref. 9), but this conclusion may not apply to material aged at lower temperatures, where the G-phase distribution will be different.

⁷S. G. Druce, unpublished research, ORNL and UKAEA, Harwell, 1988.

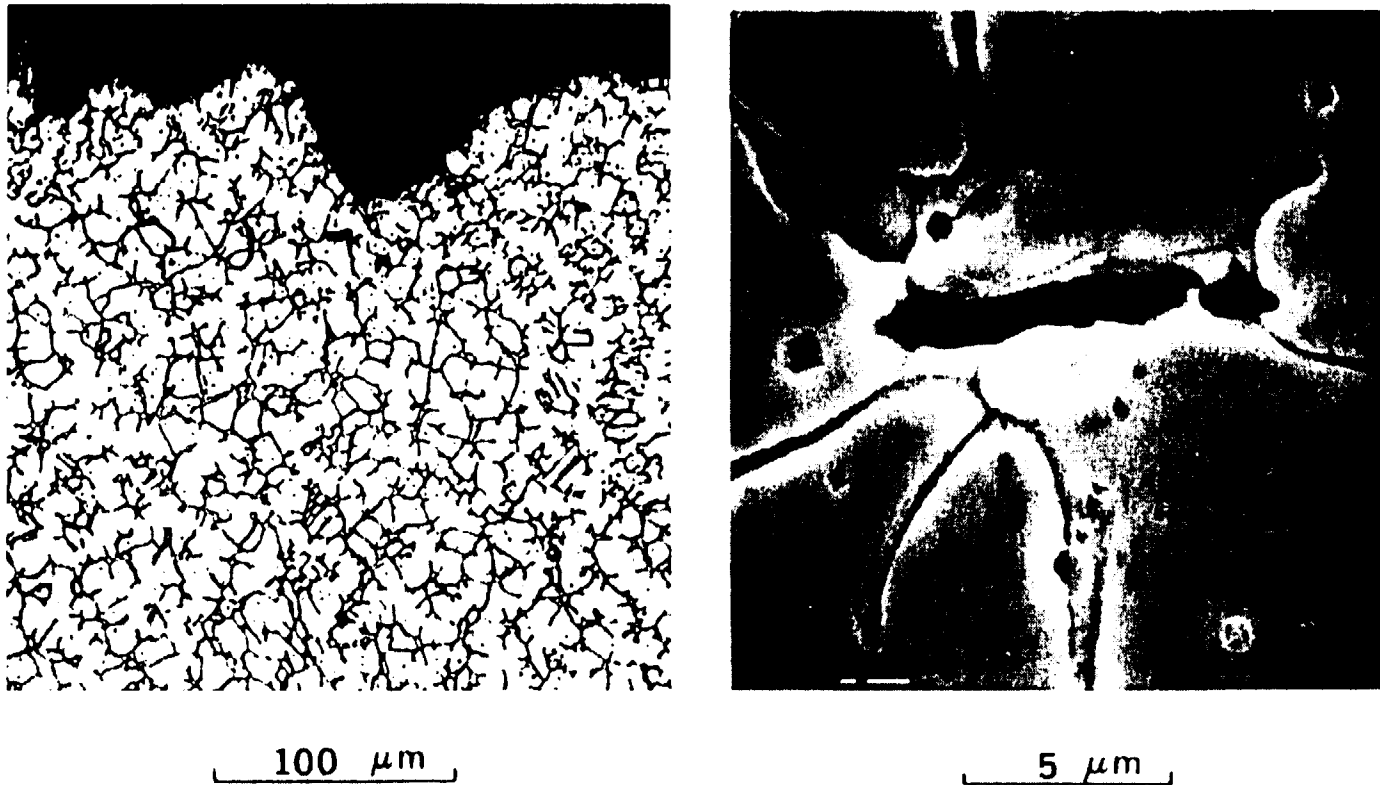


Figure 21. Section perpendicular to the fracture surface of a type 308 stainless steel weld metal Charpy impact specimen showing microcracks associated with the ferrite regions. Left: optical view of section, with microcracks indicated by arrows; right: higher-magnification SEM micrograph showing detail of microcrack in ferrite. 12% ferrite material, aged 343°C for 20,000 h, tested at -50°C.

The response of the present material to aging at 343°C differs from that due to irradiation to 5×10^{19} n/cm² (> 1 MeV) at 288°C observed by Haggag et al. (Refs. 26 and 27) on type 308 stainless steel weld overlay cladding, which has a microstructure similar to the present weld metals. They observed an increase in the transition temperature and a decrease in the upper-shelf energy level similar to that observed in the present work. Thermal aging alone at 288°C for 1605 h had little effect (Ref 28). However, the lateral expansion values are much greater in the present work, and irradiation caused a much greater relative decrease in the lateral expansion than aging caused in the present material. This may be due to the different orientation of the specimens, as Haggag et al. tested specimens of T-S orientation (crack growth perpendicular to the welding direction) as compared to the T-L orientation used in the present work (crack growth parallel to the welding direction). Additionally, irradiation would affect both the ferrite and austenite phases in the cladding material, whereas aging has apparently only altered the ferrite phase, as no changes were observed in the austenite phase. The hardening of both phases by irradiation may account for the large decrease observed on the upper-shelf lateral expansion measurements.

Chung and Chopra have shown that the mechanical properties of type CF8 alloys are largely recovered after a reversion treatment to dissolve the iron-rich and chromium-rich regions that result from spinodal decomposition (Ref. 6). Additionally, alloys with larger G-phase precipitates have been shown to possess properties similar to those with smaller precipitates (Refs. 3–5). It is therefore likely that the G-phase precipitates have a secondary influence on the mechanical properties. However, recent work on similar weldments aged at 475°C has lead to the conclusion that the G-phase plays a significant role in the degradation of the fracture properties, at least for material aged at this higher temperature (Ref. 9).

In an attempt to determine which microstructural changes are responsible for the embrittlement, a reversion heat treatment (1 h at 550°C, water quench) (Ref. 6) was used. The purpose of this heat treatment is to dissolve the spinodal decomposition without altering the G-phase distribution. The time is short enough so that carbides or other precipitates would not be expected to form. Unaged specimens and specimens from the 8 and 12% ferrite welds that had been aged 10,000 h were given the heat treatment. The results are shown in Figure 22. Impact tests were conducted at –50 and 140°C. In all cases, the reversion heat treatment caused a slight decrease in the impact energy of unaged specimens. Although it is

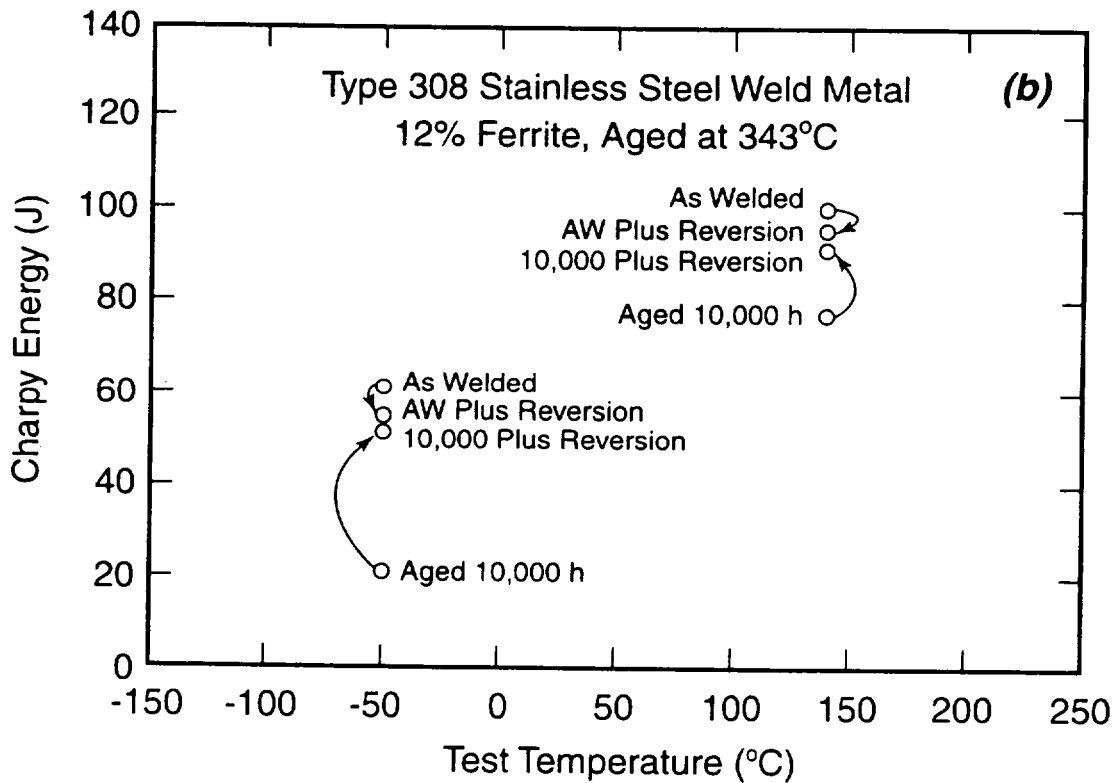
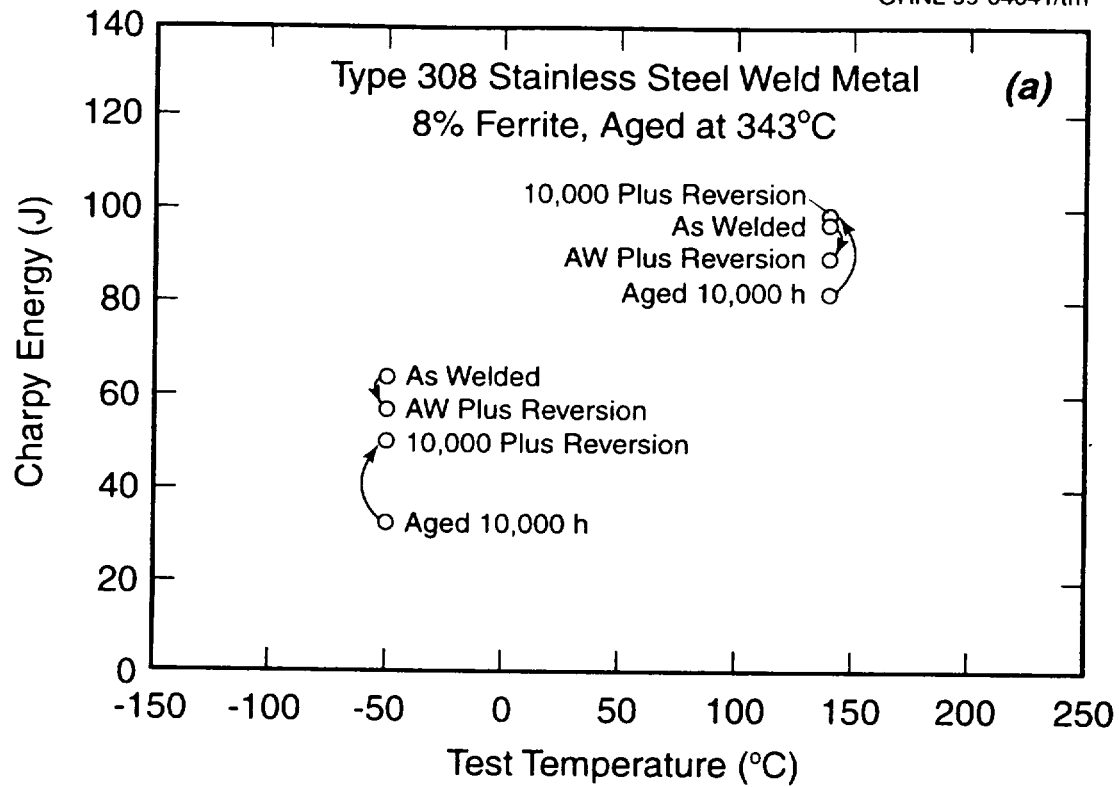


Figure 22. The effects of a reversion heat treatment (550°C for 1 h, water quench) on the impact properties of (a) 8% ferrite material and (b) 12% ferrite material, of type 308 stainless steel weld metal. Aging was performed at 343°C.

difficult to be entirely certain on the basis of only four tests, this result suggests that some changes occur in the microstructure even during the reversion heat treatment that slightly reduce the impact properties. Reversion of the aged specimens results in a significant improvement in the impact properties. The specimens show higher levels of energy absorption but usually do not fully recover to the energy levels of the unaged specimens, with the exception of the 8% ferrite material tested at 140°C. Again, although the number of tests is limited, these results suggest that the spinodal decomposition is the dominant factor in the embrittlement, but the G-phase does play a lesser, albeit important, role.

The carbides observed at the ferrite/austenite interface apparently have little influence on the fracture process. There were few carbides at the interfaces in the uppermost portion of the weld, and yet there was little difference in the impact properties as a function of location in the weld. Additionally, there is no fractographic evidence to suggest that the carbides play any significant role in the fracture process.

Although the dynamic testing indicates that there is significant embrittlement in the aged weld material, it is not clear how this would relate to in-service use. It is believed that the high strain rates encountered in the impact testing promote the occurrence of cleavage fracture in the ferrite regions of the weld metal and that aging strengthens and embrittles the ferrite, further enhancing the propensity for cleavage fracture under dynamic-loading conditions or at lower temperatures. Thus, it is the increased ease of cleavage in the aged ferrite that is responsible for the decrease in impact properties, as reflected in the increase in transition temperature with increased aging.

An increase in the volume fraction of ferrite results in greater effects of aging, as would be expected. However, it is not clear what the effects of aging will be under slow-strain-rate conditions, where the formation of cleavage cracks will be less likely, as ductile modes of failure will tend to dominate at slower strain rates, or at higher test temperatures, again where cleavage fracture is unlikely. The impact tests conducted at higher temperatures, which correspond to the upper-shelf regime, show a decrease in the upper-shelf energy level with increased aging time, an effect that is more significant as the ferrite content increases [Fig. 6(b)]. At these higher temperatures, one would expect ductile modes of fracture to occur, not cleavage, as is confirmed by SEM examination (Fig 19). This suggests that fracture

toughness tests might also show a decrease in toughness with increased aging time and increased ferrite content because these slow-strain-rate tests should also result in ductile modes of failure.

Fracture Toughness Testing

To investigate the effects of aging on fracture toughness under conditions representative of in-service use, J-Integral-resistance (J-R) curve testing was conducted on precracked Charpy V-notch (PCVN) specimens in three-point bending. The tests were conducted in general accordance with ASTM E 1737-97, Standard Test Method for J-Integral Characterization of Fracture Toughness. The specimens were precracked at room temperature and were side-grooved 20% (10% of their thickness on each side). The initial ratio of crack length to specimen width (a/W) was approximately 0.5. The maximum final stress intensity at the end of precracking was approximately $25 \text{ MPa}\sqrt{\text{m}}$. The specimens were tested on a loading rig designed for three-point bend testing of Charpy-sized specimens. The load-line displacement was measured with a linear variable differential transducer (LVDT). A rod transferred the load-line displacement from the bottom of the specimen out of the hot zone to the LVDT, which operated at room temperature. The load-line displacements were used to calculate both the energy needed for crack extension and the unloading compliance, which allowed the crack length to be calculated. All testing was conducted at 290°C , a temperature chosen as typical of in-service conditions. Both unaged specimens and those aged for 50,000 h at 343°C were tested because they would be expected to show the maximum embrittlement.

Estimated values of the yield and ultimate tensile strengths and Young's modulus and Poisson's ratio at 290°C were used for testing and analysis (310 MPa, 483 MPa, 166 GPa, and 0.3, respectively). Following heat treating and final fracturing, the crack lengths were measured on the fracture surfaces with a measuring microscope; the nine-point averaging method was used.

The results of J-R testing are shown in Fig. 23 and Table 5. The unaged material showed a high fracture toughness, essentially independent of the ferrite content. After aging for 50,000 h at 343°C , the 4% ferrite material showed no degradation of toughness, much like the upper-shelf energy results shown in Fig. 3. However, the 8 and 12% ferrite materials showed an

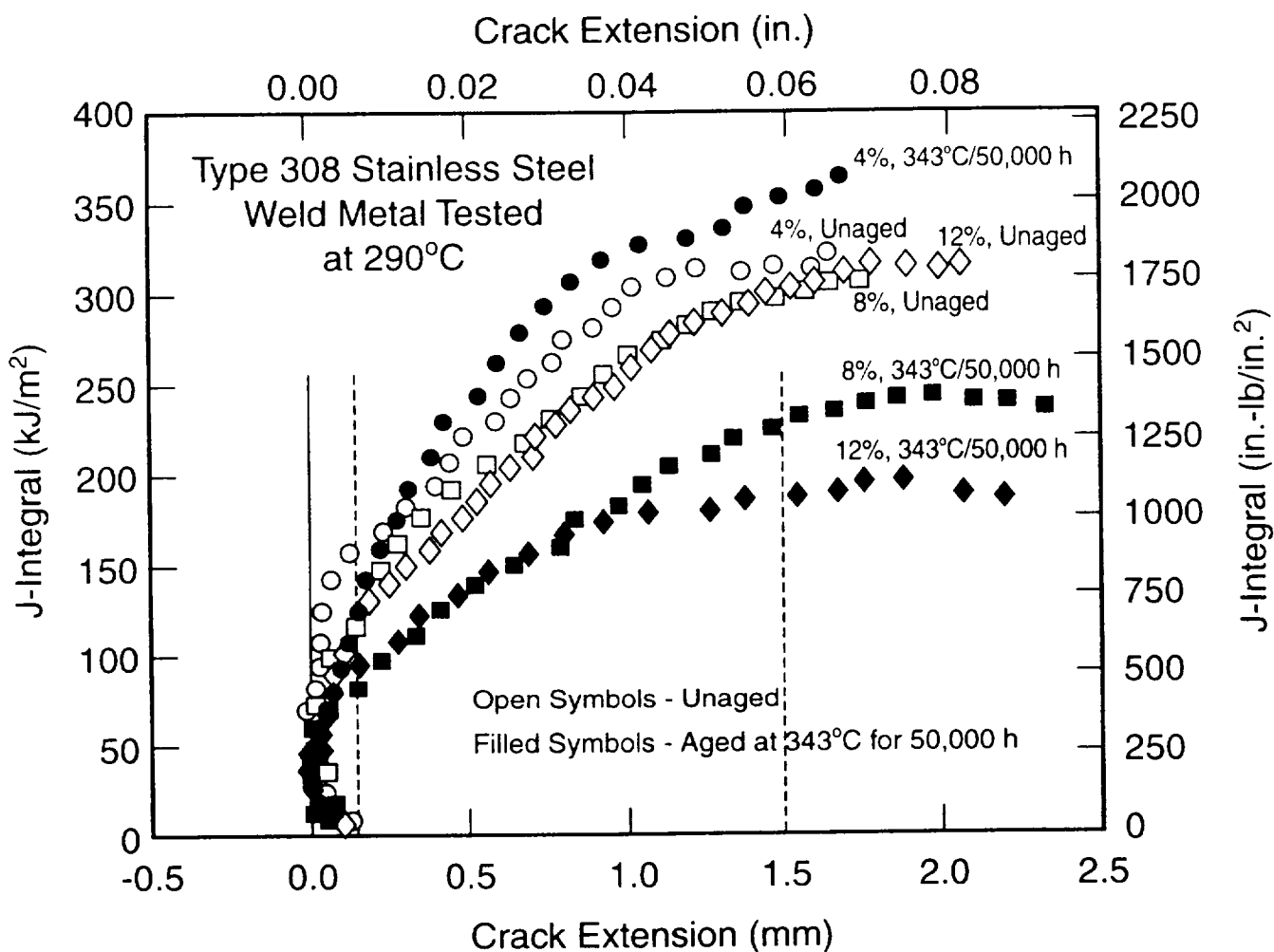


Figure 23. Effects of aging at 343°C on the J-Integral fracture toughness of type 308 stainless steel weld metal. All tests conducted with precracked Charpy V-notch specimens at 290°C.

Table 5. Effects of aging at 343°C for 50,000 h on fracture toughness of type 308 weld metal

Ferrite content (%)	Unaged			Aged 50,000 h		
	J_0 (kJ/m ²)	K_J (MPa√m)	T	J_0 (kJ/m ²)	K_J (MPa√m)	T
4	221	191	95	257	206	92
8	190	177	97	113	136	95
12	169	167	117	127	145	52

appreciable decrease in toughness, with significantly lower JQ values (Table 5), and much lower J-R curves (Fig. 23), compared with the unaged material, although even in the most embrittled condition, the toughness was still quite high. The 12% ferrite material also had a much lower tearing modulus (T), although the other materials showed little change in T.

The J-R curves of the unaged materials all tended to rise more steeply than the calculated blunting lines. This tendency is commonly observed for high-toughness, low-strength materials, such as austenitic stainless steels and their welds. After the material was aged for 50,000 h, the J-R curves showed much better agreement with the blunting lines.

The J-R curve tests showed that aging of these materials for 50,000 h at 343°C can result in an appreciable decrease in fracture toughness at 290°C for the 8 and 12% ferrite materials, although the toughness was still high. The 4% ferrite material showed little effect of aging.

The behavior of these materials in the J-R testing is very similar to that observed on the upper-shelf regime of impact testing. This similarity is not unexpected because fracture processes in both cases will occur by ductile fracture modes. The major difference between upper-shelf impact tests and the J-R fracture toughness test is the strain rate of the fracture process, which is much greater for the dynamic test conditions. However, the primarily austenitic matrix of these welds would not be expected to be strain-rate sensitive, although the ferrite portion would be. Apparently, the finely dispersed ferrite and its low volume fraction as present in these materials (a maximum of 12%) does not result in appreciable strain-rate sensitivity under conditions in which ductile fracture occurs.

The mechanism for the decrease in fracture toughness of the higher-ferrite-content materials as a result of aging for 50,000 h at 343°C is not obvious, just as is the case for the effect of aging on the upper-shelf behavior. Little effect of aging on the tensile properties at 290°C is expected, although the tensile properties were measured at only room temperature. Aging may result in subtle differences in the ductile-fracture processes in the higher-ferrite materials, but what these differences are is not apparent at present. Perhaps the higher strength of the aged ferrite results in load transfer to, and increased local strains in, the austenite matrix, which may result in earlier failure of the austenite than in the unaged metal. Further research is needed to understand the effects of aging on the ductile-fracture process.

It must be noted that none of these tests satisfy the restrictive validity limits of ASTM E 1737. In particular, most of the calculated J values greatly exceed the maximum allowable J capacity of these specimens because of the short remaining initial ligament in these PCVN specimens, and because of the low flow stress and the high toughness of these materials. In fact, the validity limit for J capacity is exceeded before the J-R data leave the blunting lines except for the most-embrittled aged 8 and 12% ferrite specimens, which just begin to depart from the blunting lines before exceeding the maximum allowable J capacity measurement limit. Furthermore, the maximum allowable crack extension is greatly exceeded for all specimens as well because the initial ligament for the precracked Charpy specimen is so short (approximately 5 mm). Nonetheless, the J-R curves do reflect the toughness of the material and do show that aging results in a significant decrease in toughness for the materials with 8 or 12% ferrite content.

CONCLUSIONS

Type 308 stainless steel welds with ferrite contents of nominally 4, 8, or 12% have been aged in air for up to 50,000 h at 343°C. Aging had a relatively small effect on the tensile properties but had a significant effect on the Charpy impact properties despite the low volume fraction of ferrite. The transition temperatures increased with aging time, and the upper-shelf energy decreased. These effects increased as the ferrite content increased and continued to increase with increasing aging time. The 12% ferrite weld exhibited a transition-temperature increase of about 60°C and a drop in upper-shelf energy of 34% after aging for 50,000 h.

Aging for 50,000 h at 343°C results in a significant decrease in the fracture toughness at 290°C of the 8 and 12% ferrite materials as measured by the J-R curve testing. There is little effect on the toughness of the 4% ferrite material. The exact mechanism responsible for this decrease in toughness is unknown.

The mechanical property results, along with the microstructural evidence, indicate a hardening of the ferrite. The aged ferrite contains both heterogeneously and homogeneously nucleated G-phase and has also undergone phase separation by spinodal decomposition into iron-rich

and chromium-rich regions. These changes result in hardening of the ferrite. The increase in the transition temperature is believed to be due to the increased ease of cleavage initiation in the aged ferrite. Increasing the amount of ferrite makes crack propagation easier and increases the effects of aging on the impact properties. Reversion heat treatment results indicate that the spinodal decomposition of the ferrite rather than the G-phase precipitation is the primary cause of the hardening of the ferrite, and thus the property degradation in these materials upon aging.

REFERENCES

1. A. Trautwein and W. Gysel, "Influence of Long-Time Aging of CF8 and CF8M Cast Steel at Temperatures Between 300 and 500°C on Impact Toughness and Structural Properties," pp. 165–89 in *Stainless Steel Castings, ASTM STP 756*, V. G. Behal and A. S. Melilli, Eds., American Society for Testing and Materials, Philadelphia, 1982.*
2. M. Prager, Ed., *Properties of Stainless Steels in Elevated Temperature Service*, MPC-Vol. 26, PVP-Vol. 132, American Society of Mechanical Engineers, New York, 1988.*
3. M. K. Miller and J. Bentley, "APFIM and AEM Investigation of CF8 and CF8M Primary Coolant Pipe Steels," *Mat. Sci. and Technol.* **6**, 285–92 (1990).*
4. J. Bentley and M. K. Miller, "Combined Atom Probe and Electron Microscopy Characterization of Fine-Scale Structures in Aged Primary Coolant Pipe Stainless Steel," *Mat. Res. Symp. Proc.* **82**, 163–68 (1987).*
5. M. K. Miller and J. Bentley, "Microstructural Characterization of Primary Coolant Pipe Steel," *J. de Phys.* **47-C7**, 239–44 (1986).*

6. H. M. Chung and O. K. Chopra, "Long-Term Aging Embrittlement of Cast Austenitic Stainless Steels—Mechanism and Kinetics," pp. 17–34 in *Properties of Stainless Steels in Elevated Temperature Service*, M. Prager, Ed., MPC-Vol. 26, PVP-Vol. 132, American Society of Mechanical Engineers, New York, 1988.*
7. J. M. Vitek, "G-Phase Formation in Aged Type 308 Stainless Steel," *Met. Trans. A* **18A**, 154–56 (1987).*
8. J. M. Vitek and S. A. David, "The Aging Behavior of Types 308 and 308CRE Stainless Steels and Its Effect on Mechanical Properties," p. 157 in *Properties of Stainless Steels in Elevated Temperature Service*, M. Prager, Ed., MPC-Vol. 26, PVP-Vol. 132, American Society of Mechanical Engineers, New York, 1988.*
9. J. M. Vitek, S. A. David, D. J. Alexander, J. R. Keiser, and R. K. Nanstad, "Low Temperature Aging Behavior of Type 308 Stainless Steel Weld Metal," *Acta Metall. Mater.* **31(4)**, 503–16 (1991).*
10. D. J. Alexander, K. B. Alexander, and R. K. Nanstad, "The Effect of Aging at 343°C on Type 308 Stainless Steel Welds," pp. 217–21 in *Recent Trends in Welding Science and Technology TWR'89*, S. A. David and J. M. Vitek, Eds., ASM International, Materials Park, Ohio, 1990.*
11. D. J. Alexander, K. B. Alexander, M. K. Miller, and R. K. Nanstad, "The Effect of Aging at 343°C on 308 Stainless Steel Weldments," pp. 187–92 in *Fatigue, Degradation and Fracture*, PVP-Vol. 195, W. H. Bamford, C. Becht IV, S. B. Framatome, J. D. Gilman, L. A. James, and M. Prager, Eds., American Society of Mechanical Engineers, New York, 1990.*
12. K. B. Alexander, M. K. Miller, D. J. Alexander, and R. K. Nanstad, "Microscopical Evaluation of Low-Temperature Aging of Type 308 Stainless Steel Weldments," *Mat. Sci. Tech.* **6**, 314–20 (1990).*

13. D. J. Alexander, K. B. Alexander, M. K. Miller, and R. K. Nanstad, "The Effect of Aging at 343°C on the Mechanical Properties and Microstructure of Type 308 Stainless Steel Weldments," pp. 263–69 in *Microstructures and Mechanical Properties of Aging Materials*, P. K. Liaw, R. Viswanathan, K. L. Murty, E. P. Simonen, and D. Frear, Eds., The Minerals, Metals and Materials Society, Warrendale, Pa., 1993.*
14. D. J. Alexander and R. K. Nanstad, "The Effects of Aging for 50,000 Hours at 343°C on the Mechanical Properties of Type 308 Stainless Steel Weldments," pp. 747–58 in *Seventh International Symposium on Environmental Degradation of Materials in Nuclear Power Systems—Water Reactors*, Vol. 2, NACE International, Houston, 1995.*
15. M. K. Miller, "The ORNL Atom Probe," *J. de Phys.* **47-C2**, 493–98 (1986).*
16. M. K. Miller, "Ultrahigh Resolution Chemical Analysis with the Atom Probe," *Int. Mater. Rev.* **32**, 221–40 (1987).*
17. K. B. Alexander, P. Angelini, and M. K. Miller, "Precision Ion Milling of Field-Ion Specimens," *J. de Phys.* **50-C8**, 549–54 (1989).*
18. C. A. Johnson and J. H. Klotz, "The Atom Probe and Markov Chain Statistics of Clustering," *Technometrics* **16**, 495 (1974).*
19. M. G. Hetherington and M. K. Miller, "On the Statistical Analysis of Atom Probe Data," *J. de Phys.* **48-C6**, 559–64 (1987).*
20. J. M. Sassen, M. G. Hetherington, T. J. Godfrey, G. D. W. Smith, P. H. Pumphrey, and K. N. Akhurst, "Kinetics of Spinodal Reaction in the Ferrite Phase of a Duplex Stainless Steel," pp. 65–78 in *Properties of Stainless Steels in Elevated Temperature Service*, M. Prager, Ed., American Society of Mechanical Engineers, New York, 1987.*
21. T. J. Godfrey, M. G. Hetherington, J. M. Sassen, G. D. W. Smith, "The Characterization of Spinodal Structures in Duplex CF3 Steels," *J. de Phys.* **49-C6**, 421–26 (1988).*

22. M. G. Hetherington and M. K. Miller, "Statistical Analysis of the Early Stages of Phase Decomposition," *J. de Phys.* **49-C6**, 427–32 (1988).*
23. S. S. Brenner, M. K. Miller, and W. A. Soffa, "Spinodal Decomposition of Iron-32 at. % Chromium at 470°C," *Scripta Metall.* **16**, 831–36 (1982).*
24. W. C. Oliver and G. M. Pharr, "An Improved Technique for Determining Hardness and Elastic Modulus Using Load and Displacement Sensing Indentation Experiments," *J. Mater. Res.* **7(6)**, 1564–83 (June 1992).*
25. D. J. Alexander and G. M. Goodwin, "Thick-Section Weldments in 21-6-9 and 316LN Stainless Steel for Fusion Energy Applications," *J. Nucl. Mater.* **191–194**, 691–95 (1992).*
26. F. M. Haggag, W. R. Corwin, D. J. Alexander, and R. K. Nanstad, "Tensile and Charpy Impact Behavior of an Irradiated Three-Wire Series-Arc Stainless Steel Cladding," pp. 361–72 in *Effects of Radiation on Materials: 14th International Symposium (Vol. II)*, ASTM STP 1046, N. H. Packan, R. E. Stoller, and A. S. Kumar, Eds., American Society for Testing and Materials, Philadelphia, 1990.*
27. F. M. Haggag, W. R. Corwin, and R. K. Nanstad, "Effects of Irradiation on the Fracture Properties of Stainless Steel Weld Overlay Cladding," *Nucl. Eng. Des.* **124**, 129–41 (1990).*
28. F. M. Haggag and R. K. Nanstad, "Effects of Thermal Aging and Neutron Irradiation on the Mechanical Properties of Stainless Steel Weld Overlay Cladding," pp. 327–32 in *Fifth International Symposium on Environmental Degradation of Materials in Nuclear Power Systems—Water Reactors*, American Nuclear Society, La Grange Park, Ill., 1992.*

*Available in public technical libraries.

BIBLIOGRAPHIC DATA SHEET

(See instructions on the reverse)

1. REPORT NUMBER
(Assigned by NRC, Add Vol., Supp., Rev.,
and Addendum Numbers, if any.)

NUREG/CR-6628
ORNL/TM-13767

2. TITLE AND SUBTITLE

The Effect of Aging at 343°C on the Microstructure and Mechanical Properties of Type 308 Stainless Steel Weldments

3. DATE REPORT PUBLISHED

MONTH YEAR
November 2000

4. FIN OR GRANT NUMBER

5. AUTHOR(S)

D. J. Alexander, K. B. Alexander, M. K. Miller, R. K. Nanstad, and Y. A. Davidov

6. TYPE OF REPORT

W6953

7. PERIOD COVERED (Inclusive Dates)

Technical

8. PERFORMING ORGANIZATION - NAME AND ADDRESS (If NRC, provide Division, Office or Region, U.S. Nuclear Regulatory Commission, and mailing address; if contractor, provide name and mailing address.)

Oak Ridge National Laboratory
Oak Ridge, TN 37831-6285

9. SPONSORING ORGANIZATION - NAME AND ADDRESS (If NRC, type "Same as above"; if contractor, provide NRC Division, Office or Region, U.S. Nuclear Regulatory Commission, and mailing address.)

Division of Engineering Technology
Office of Nuclear Regulatory Research
U.S. Nuclear Regulatory Commission
Washington, D.C. 20555-0001

10. SUPPLEMENTARY NOTES

C. J. Fairbanks, NRC Project Manager

11. ABSTRACT (200 words or less)

Some piping systems in light-water reactors contain welds made with type 308 stainless steel filler metal that are routinely subjected to operating temperatures above 300°C. The effect of long-term aging of stainless steel welds at 343°C (650°F) has been studied by the Heavy-Section Steel Irradiation Program to determine the extent of degradation of the mechanical properties of the weld metal. Three multipass shielded metal-arc welds were prepared from type 304L base plate with type 308 filler metal. Portions of these welds were aged for 3,000, 10,000, 20,000 or 50,000 h at 343°C. The tensile results were similar for all the specimens and showed little effect of aging on the yield or ultimate tensile strength or the ductility. In contrast, the Charpy impact toughness, as characterized by either the ductile-to-brittle transition temperature or the upper-shelf energy, was significantly degraded by aging. The extent of the degradation increased with increasing ferrite content and increasing aging time. Embrittlement continued to increase up to 50,000 h of aging with no indication of a saturation. The microstructures of the welds were examined by optical metallography, scanning and transmission electron microscopy, and atom probe field-ion microscopy. Examination of material aged for 20,000 h showed that the ferrite phase undergoes spinodal decomposition, creating iron-rich and chromium-rich regions. No changes were observed in the austenite phase. The hardening of the ferrite phase due to the spinodal decomposition is believed to be the primary factor responsible for the loss of toughness observed after aging.

12. KEY WORDS/DESCRIPTORS (List words or phrases that will assist researchers in locating the report.)

thermal aging
atom probe field ion microscopy
Charpy V-notch
G-phase
electron microscopy

stainless steel weldments
tensile strength
fracture toughness
spinodal decomposition

13. AVAILABILITY STATEMENT

Unclassified

14. SECURITY CLASSIFICATION

(This Page)

Unclassified

(This Report)

Unclassified

15. NUMBER OF PAGES

16. PRICE



Federal Recycling Program

UNITED STATES
NUCLEAR REGULATORY COMMISSION
WASHINGTON, D.C. 20555-0001

